CT and MRI of the Orbit

Andrew S. Griffin, MD
Jenny K. Hoang, MBBS, MHS
Michael D. Malinzak, MD, PhD

Computed Tomography (CT) Imaging for Orbital Pathology

CT imaging is produced by obtaining radiographic images in multiple projections using a revolving x-ray tube and x-ray detector. Modern CT technology allows for the rapid acquisition of high-quality data that can be used to create a variety of image types from a single scan. Multidetector CT scanners, which have become common place, yield volumetric data thus allowing for images to be reconstructed in any plane of view (typically coronal and sagittal planes in addition to the axial plane of data acquisition).

Different reconstruction algorithms are used to produce the viewable images at the level of the scanner, and both soft tissue and bone algorithms are applied for CT examinations of the orbits. Images reconstructed using a soft tissue algorithm have less noise and provide better contrast resolution for distinguishing subtle differences in radiodensity among soft tissue structures. Images reconstructed using a bone algorithm exhibit more noise but provide better spatial resolution for identifying defects and internal architectural features of bony structures. It is common, but not necessary, to apply the soft tissue algorithm to thicker cut images (further reducing image noise), and to apply the bone algorithm to thin cut images (further increasing spatial resolution). The end result for the imaging user is 2 sets of images in each plane, optimized for assessment of different structures, thereby reviewed with these different purposes in mind.

Our imaging protocol here at Duke for CT of the orbits begins with the acquisition of axial CT data from above the level of the frontal sinuses to the level of the hard palate. Axial, coronal, and sagittal plane reconstructions are then made using 0.625 mm slice thickness in bone

INTERNATIONAL OPHTHALMOLOGY CLINICS
Volume 58, Number 2, 25–59

algorithm, and 1.25 mm slice thickness in soft tissue algorithm for a total of 6 series of images.

CT studies of the orbits can be performed without or with contrast enhancement. Contrast-enhanced CT of the orbits is obtained following the intravenous (IV) administration of an iodinated contrast agent in venous phase (Fig. 1). If there is concern for an orbital mass, contrast-enhanced CT is preferred because a variety of common orbital pathologies exhibit characteristic enhancement patterns. CT without contrast enhancement is sufficient for orbital trauma or thyroid orbitopathy as these pathologies are very well outlined by hypoattenuating intraorbital fat. Importantly, CT of

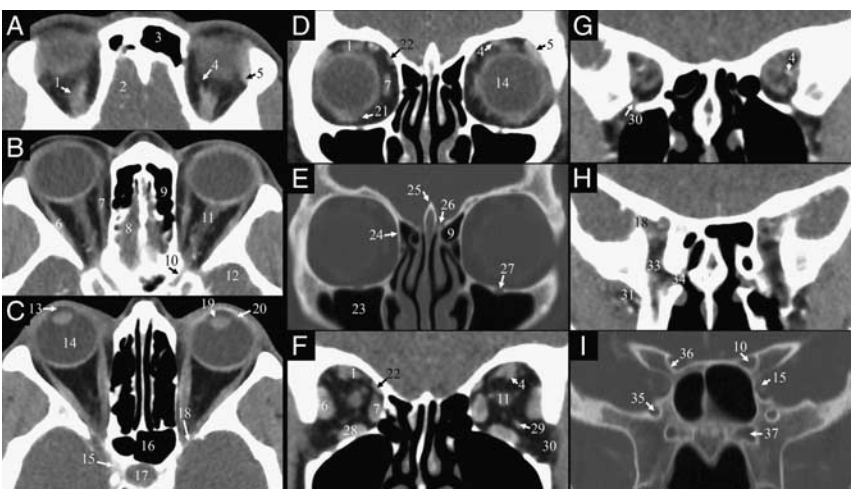

Figure 1. *A–C, Axial contrast-enhanced CT images of the orbits progressing from superior to inferior. A, Image through the superior orbits demonstrates the levator palpebrae and superior rectus muscles (1) which are often not clearly delineated from each other, the frontal lobe (2), frontal sinus (3), enhancing superior ophthalmic vein (4), and enhancing lacrimal gland (5). B, Image through the mid orbits demonstrates the enhancing lateral rectus muscle (6), enhancing medial rectus muscle (7), olfactory bulb (8), ethmoid air cells (9), optic canal (10), intraorbital optic nerve (11), and temporal lobe (12). C, Image through a more inferior portion of the mid orbits shows the anterior segment of the eye (13), vitreous body (14), enhancing cavernous sinus (15), sphenoid sinus (16), pituitary fossa (17), superior orbital fissure (18), lens (19), and ciliary body (20). D–I, Coronal contrast-enhanced CT images of the orbits progressing from anterior to posterior. D, Image through the anterior orbits on soft tissue window demonstrates the enhancing extraocular muscles including the inferior oblique (21) and superior oblique (22). E, Image through the anterior orbits on bone window demonstrates the maxillary sinus (23), lamina papyracea (24), crista galli (25), cribriform plate (26), and infraorbital canal (27). F, Image through the mid orbits shows the enhancing extraocular muscles including the inferior rectus (28), as well as the enhancing inferior ophthalmic vein (29) and inferior orbital fissure (30). G, Image through the anterior orbital apex shows the converging extraocular muscles with a portion of the inferior orbital fissure (30) and the conspicuously enhancing superior ophthalmic vein (4). H, Image at the level of the posterior orbital apex shows the masticator space (31), superior orbital fissure (18), pterygopalatine fossa (33), and sphenopalatine foramen (34). I, Image through the optic canals (10) shows the foramen rotundum (35), optic strut forming the floor of the optic canal (36), cavernous sinus (15), and Vidian canal (37). CT indicates computed tomography.*

the orbits is not typically performed both without and with contrast enhancement; this technique doubles radiation dose to the ocular lens without significantly improving diagnostic yield.

■ Magnetic Resonance Imaging (MRI) for Orbital Pathology

MRI is produced by placing a patient within a strong magnetic field and applying a variety of superimposed magnetic gradients and radiofrequency pulses. These actions cause protons within tissues to emit radiofrequency signals, which are detected and used to infer the locations and chemical environments of the protons. The order and timing of magnetic gradient application, radiofrequency pulse application, and radiofrequency recording characterizes the imaging acquisition sequence (eg, T1 or T2-weighted imaging). Different sequences produce different signal characteristics for different tissues, such that water—for example—will reliably exhibit signal hyperintensity (ie, appear bright) on a T2-weighted imaging sequence.

By examining the signal characteristics of a tissue on multiple sequences, the image interpreter can infer chemical and physiological properties of the tissue to varying degrees of certainty. Although a great number of sequences are available, the acquisition of each sequence takes time, and therefore only a tailored set of sequences is obtained in a given MRI orbits protocol. Commonly used sequences in MRI of the brain and orbits include T1-weighted, T1-weighted fat-saturated, T1-weighted contrast-enhanced, T2-weighted, T2-weighted fat-saturated, fluid attenuation inversion recovery (FLAIR), diffusion weighted imaging (DWI), and susceptibility weighted imaging (SWI).

On T1-weighted images, fat appears bright, myelin appears bright gray, muscle and glandular tissue appears dark gray, and water appears dark. Following the IV administration of gadolinium-based contrast agents, T1-weighted contrast-enhanced images typically appear bright in regions of higher gadolinium concentration such as highly vascular mucosa, muscle, or tumor. On T2-weighted images, fat again appears bright, water appears bright, glandular tissue appears bright gray, and myelin and muscle appear dark gray. Blood varies in signal on T1 and T2-weighted images depending on its rate of flow, degree of erythrocyte integrity, and iron oxidation state. Calcified structures have low proton density, and so appear dark on both T1 and T2-weighted imaging.

Saturation is a term used to refer to the nulling of signal from a particular tissue type. This is typically performed to increase the conspicuity of one source of bright signal when it superimposed on a background tissue that also exhibits bright signal; for example, allowing for the identification of bright edema/water within orbital fat on T2-weighted images. Consequently, fat-saturated T1 and T2-weighted

images exhibit the same signal characteristics as listed above except that fat (and lipid-rich myelin) now exhibits low signal on both. FLAIR can be thought of as T2-weighted imaging in which the signal from macroscopic water has been nulled or saturated out, particularly useful for identifying edema within the brain. Unfortunately, all saturation techniques are prone to failure, and failed or inhomogenous signal saturation produces a variety of bright-appearing artifacts easily mistaken for contrast enhancement or edema.

DWI uses strong magnetic gradients to produce images wherein decreased Brownian motion of water, such as is commonly caused by swollen or densely packed cells, produces bright signal. As a result, restricted diffusion can imply highly cellular tumor such as lymphoma, thick pus, or—when observed in the brain parenchyma or optic nerves—acute infarct. A variety of other entities, such as hemorrhage and magnetic field inhomogeneities, produce high signal on DWI. SWI is used to visualize chemicals that produce magnetic field inhomogeneity. Thrombus and calcium variably appear bright or dark, whereas hemosiderin uniformly appears dark on SWI.

The default protocol for MRI of the orbits is to obtain both unenhanced and enhanced imaging. Unenhanced MRI of the orbits is performed alone only when there is a contraindication to IV gadolinium agent administration (eg, pregnancy, contrast allergy, or renal failure). At Duke, MRI of the orbits is almost exclusively acquired in conjunction with MRI of the brain. Images are obtained on a 3 T magnet using a 20 channel dedicated head/neck coil. Using 5 mm slice thickness, axial T1, axial T1 contrast-enhanced, axial T2, axial FLAIR, axial DWI, and sagittal T2-weighted images are obtained for the brain. Using 2.5 or 3.0 mm slice thickness, axial T1, axial T1 fat-saturated contrast-enhanced, coronal T1, coronal T1 fat-saturated contrast-enhanced, and coronal T2 fat-saturated images are obtained with the eyes closed (Fig. 2). This standard MRI protocol for the brain and orbits takes just under 30 minutes to complete. A variety of additional brain imaging sequences are added depending on the clinical context: sagittal FLAIR in the setting of suspected demyelinating disease, SWI in the setting of suspected stroke, thin cut axial T1-weighted unenhanced and contrast-enhanced images in the setting of suspected brain mass, and a 3D heavily T2-weighted steady state free precession image of the posterior fossa for cranial nerve cisternal segment abnormalities.

■ Vascular Imaging for Orbital Abnormalities

Certain ophthalmologic presentations can raise suspicion for underlying vascular lesions including carotid stenosis, intracranial aneurysm, venous thrombosis, carotid cavernous fistula (CCF), orbital varix, and orbital vascular malformation. In this setting, dedicated cross-sectional

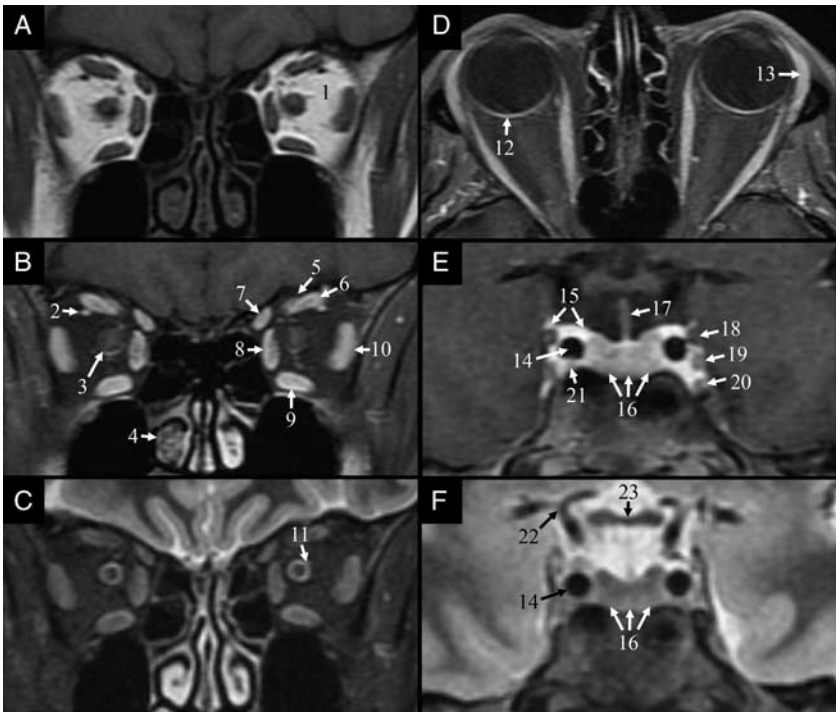

Figure 2. *A, Coronal T1-weighted noncontrast-enhanced image through the mid orbits demonstrates normal anatomy; note the homogenous signal displayed by normal intraconal fat (1). B, Coronal T1-weighted contrast-enhanced fat-saturated image through the mid orbits demonstrates the enhancing superior ophthalmic vein (2), normal subtle enhancement of the optic nerve (3), and normal enhancement of the nasal mucosa which is often asymmetric (4). Also at this level, normal avid enhancement of the extraocular muscles is demonstrated including the levator palpebrae (5), superior rectus (6), superior oblique (7), medial rectus (8), inferior rectus (9), and lateral rectus (10). C, Coronal T2-weighted fat-saturated image through the mid orbits demonstrates normal signal intensity of the extraocular muscles as well as a layer of CSF within the optic nerve sheath, which can vary in thickness (11). D, Axial T1-weighted contrast-enhanced fat-saturated image through the mid orbits demonstrates the normal thin enhancing appearance of the ocular choroid (12) and the normal strong enhancement of the lacrimal gland (13). E, Coronal T1-weighted contrast-enhanced fat-saturated image through the cavernous sinus demonstrates the normal cavernous ICA flow void (14), normal enhancement in the cavernous sinus (15), normal hypoenhancement of the pituitary gland (16) relative to the adjacent cavernous sinus, and normal enhancement of the pituitary infundibulum (17) which appears bright compared to the surrounding CSF. Also at this level, several cranial nerves are inconstantly visible with nerves III-IV (18), V1 (19), and V2 (20) along the lateral margin of the cavernous sinus and nerve VI (21) faintly visible in its more medial location. F, Coronal T2-weighted fat-saturated image through the cavernous sinus shows the ICA terminus (22), normal cavernous ICA flow void (14), and pituitary gland (16) which appears hypointense relative to adjacent cavernous sinus and CSF. The optic chiasm (23) is also well seen at this level and normally exhibits low signal intensity due to its high myelin content. CSF indicates cerebrospinal fluid.*

vascular imaging using CT or MR angiography is usually the initial step in the evaluation. Conventional angiography provides better temporal resolution, evaluation of flow direction, and the best spatial resolution of

any angiographic technique. However, the invasive nature of conventional angiography and attendant increased risk of complications including arterial bleeding and stroke has led to selective use of this modality. In particular, conventional angiography is used as a problem-solving tool when first-line CT or MR angiography results are unclear, or for intraprocedural guidance of catheter-directed therapies.

CT angiography techniques for CT arteriography (CTA) and CT venography (CTV) both are dependent on IV administration of the iodinated contrast. Appropriate contrast bolus timing is critical, particularly for CTA as the phase of maximum arterial enhancement without venous contamination is short lived. Power injection of iodinated contrast is required for CTA, with a goal rate of 4 to 5 mL/s, but this is not necessary for CTV. Typically, automatic bolus timing is used in CTA, wherein low-radiation images are repeatedly obtained at the aortic arch, and automatic measurements of attenuation in the aortic blood pool are used to identify the beginning of arterial phase and to trigger image acquisition.

Both MR arteriography (MRA) and MR venography (MRV) can be performed using either contrast-enhanced or unenhanced time-of-flight (TOF) techniques. In the cervical vessels, the high rate and turbulent nature of blood flow produce artifacts on TOF-simulating stenosis or occlusion. As a result, contrast-enhanced MRA is our preferred MR technique for imaging the neck vessels. At the circle of Willis, contrast-enhanced MRA is very prone to unintended visualization of venous enhancement, and so TOF MRA (which routinely includes saturation of downward flowing venous blood signal) is the preferred method for examining the large intracranial arteries. MRV for assessment of venous sinus thrombosis is prone to artifactual nonvisualization of certain vessel segments when using TOF technique. The presence of arachnoid granulations within the dural sinuses, and the high incidence of developmental intracranial venous asymmetry can further confound interpretation. As a result, contrast-enhanced MRV is often performed independently or in conjunction with TOF MRV for patients who have no contraindication to IV gadolinium contrast agents.

Comparing the 2 modalities, the drawbacks of MRA/MRV are their propensity for artifacts and lower spatial resolution than CTA/CTV; whereas, the drawbacks of CTA/CTV are the absolute requirement for IV contrast medium administration and the use of ionizing radiation. For these reasons, we prefer to use MRA a screening tool for patients with low pretest probability of aneurysm or stenosis, to follow treated lesions that will require frequent repeat imaging such as aneurysms, or to evaluate lesions best evaluated with multiphase contrast-enhanced imaging techniques such as vascular malformations. CTA is preferred for the initial evaluation in patients suspected to have carotid stenosis, CCF, or an intracranial aneurysm. Venous sinus thrombosis may be associated with intraparenchymal hemorrhage and venous infarction. The information regarding the brain parenchyma gained by performing anatomic

MRI in conjunction with MRV is offset by the propensity for the MRV to exhibit artifacts. As a result, we have no strong preference for performing a MRV versus CTV in a patient with possible venous sinus thrombosis.

■ Practical Tips for Choice of Image Modality

The choice of MR versus CT is an important decision for the ophthalmologist evaluating a suspected disease of the orbit. This decision is impacted by patient factors such as contraindications to contrast agents and claustrophobia, sometimes by logistic issues such as MR availability, as well as by the suspected acuity and differential diagnosis. Although the information provided by CT and MR of the orbits overlaps to a degree, the modalities have different strengths and there can be value to performing both in select cases.

MRI brain and orbits without and with contrast is preferred for the majority of orbital pathologies, particularly for patients with subacute or chronic disease on presentation MRI is preferred to CT in the evaluation of suspected orbit neoplasms, orbit inflammatory disorders, orbit vascular malformations (consider adding MRA head), demyelinating processes, ischemia (consider adding MRA head and neck), CCF (add MRA head), cranial nerve abnormalities, evidence of increased intracranial pressure (add MRV head), and brain mass lesions.[1,2]

CT can be used to complement MRI for certain orbital pathologies. In particular, CT demonstrates calcium and air far better than MRI. As a result, unenhanced CT can be helpful to confirm characteristic tumor calcification patterns such as those encountered with retinoblastoma, optic nerve sheath meningioma, and osseous processes such as fibrous dysplasia. Its ability to characterize the air-filled paranasal sinuses renders CT the test of choice for suspected spread of bacterial sinus infection to the orbits.[1] CT's wide availability, short time required for image acquisition, and excellent visualization of fractured bone and extravasated blood also make it the first-line study for evaluating critically ill and trauma patients.

■ Orbital Trauma

Orbital trauma is a commonly encountered scenario in the emergency department. Prompt diagnosis and treatment can be essential to avoid cosmetic deformity and visual impairment. Clinical evaluation of eye injuries is often challenging in the acute setting due to soft tissue swelling and altered consciousness, and therefore imaging plays a central role in the evaluation of orbital trauma. CT has emerged as the best initial imaging test because it is a readily available modality, fast to perform, sensitive for the detection of fractures and foreign bodies, and allows for assessment of adjacent injuries.

Orbital Blowout Fractures

Orbital fractures can be described as blow-in, blowout, or blown up fractures with the name reflecting the direction of fracture and displacement of orbital contents. Blowout fractures imply herniation of soft tissues outside the orbit and are typically divided into pure and impure forms; they are considered pure if the orbital rim is spared and impure if the orbital rim is involved.[3] Orbital fractures may be isolated or combined with other maxillofacial fractures such as Le Fort II and III fractures as well as zygomaticomaxillary and nasoethmoid fractures. Fracture of the inferior orbital wall is the most common type of blowout fracture, followed by fracture of the medial wall (Fig. 1). These fractures can affect globe position and extraocular muscle movement resulting in visual problems such as diplopia and enophthalmos.[4] One of the most significant consequences of orbital wall fracture is muscle herniation (Fig. 3). Large volume fat herniation can also cause traction of the muscle and lead to symptoms which may be an indication for urgent surgery.[5,6] Orbital edema and hemorrhage as well as cranial nerve injury can also adversely affect movement of the globe.

Orbital Hemorrhage

Orbital hemorrhage is a potential complication of trauma, particularly when there is an orbital or facial fracture present.[7] Retrobulbar hemorrhage is

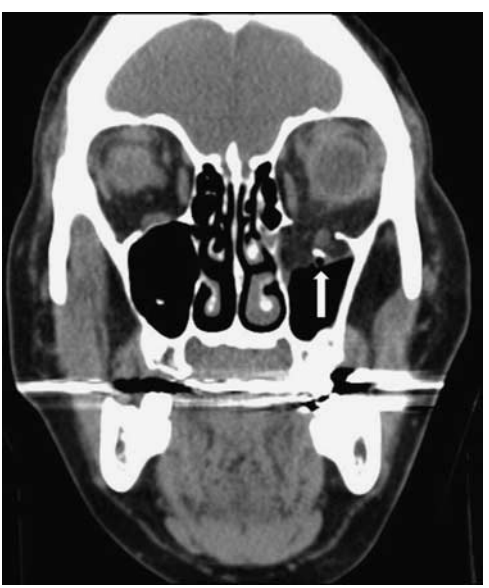

Figure 3. *31-year-old woman sustained a motor vehicle accident. A coronal computed tomographic image through the orbits demonstrates a blowout fracture of the left orbit with a displaced fracture of the inferior orbital floor. There is herniation of intraorbital fat and the inferior rectus muscle into the maxillary sinus (white arrow).*

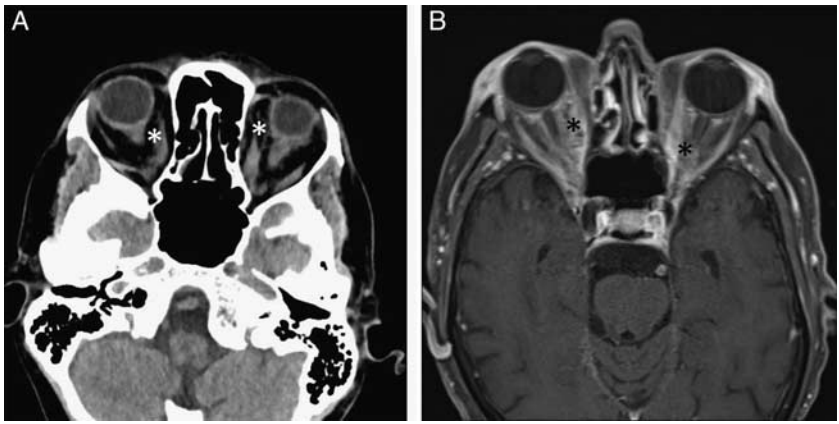

Figure 4. *76-year-old man presented to the emergency department after being stabbed in both eyes with screw drivers. An axial computed tomographic image through the level of the orbits demonstrates ill-defined high attenuation within the intraconal spaces consistent with hemorrhage (A, white asterisks). An axial T1-weighted magnetic resonance imaging through the level of the orbits in the same patients demonstrates ill-defined T1 hyperintensity in the intraconal spaces (B, black asterisks).*

an accumulation of blood in the retrobulbar space and often results from injury to the infraorbital artery or one of its branches.[8] Although the incidence is relatively low, ranging from 1% to 4% after trauma, they are important to recognize because they can rapidly lead to permanent vision loss.[9] The orbit is a fixed space with no significant ability to expand, making it vulnerable to compartment syndrome. An acute rise in orbital volume from even a small amount of hemorrhage can increase the orbital pressure and result in decreased perfusion of the optic nerve and retina, resulting in ischemia and permanent vision loss.[10] Retrobulbar hemorrhage is identified on CT as ill-defined high attenuation within the soft tissues posterior to the globe (Fig. 4A). On MRI, acute hemorrhage will appear T1 hyperintense (Fig. 4B).

■ Orbital Vascular Lesions

According to the International Society for the Study of Vascular Anomalies (ISSVA) vascular lesion are classified into 2 broad categories: vascular tumors and vascular malformations.[11] Vascular tumors are true neoplasms and grow by endothelial hyperplasia. Vascular malformations have quiescent endothelium and are considered localized defects of vascular morphogenesis. Vascular malformations can be classified as simple capillary, venous, lymphatic or arteriovenous, or a combination of these components.

Orbital Venous Varix

Orbital varices are venous malformations that are distensible and most commonly present as unilateral intermittent proptosis in the second or third

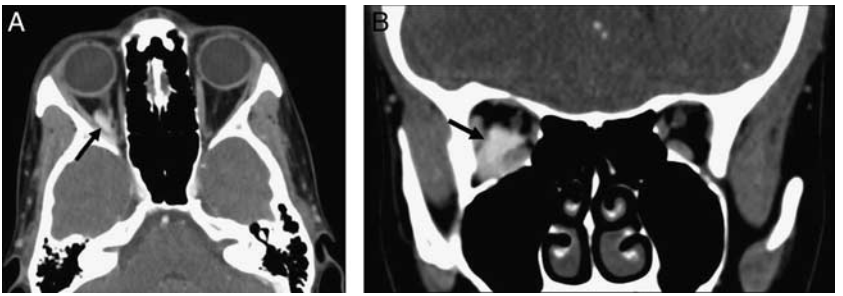

Figure 5. *34-year-old woman presented with positional right periorbital pain. Patient was imaged during a Valsalva maneuver. Axial (A) and coronal (B) images of a contrast-enhanced computed tomography through the level of the orbits demonstrates an enhancing tubular structure in the right orbital apex consistent with a varix (black arrows).*

decade of life.[12] Patients classically report worsening of proptosis with maneuvers that increase venous pressure such as Valsalva or lowering of the head. Orbital varices typically arise from the superior ophthalmic vein and are thought to be due to a congenital weakness in the venous wall.[13] Varices may be evaluated with ultrasonography (US), CT, or MRI. On US, varices appear as an anechoic retrobulbar tubular structure.[14] If imaged during a Valsalva maneuver, the lesion will enlarge and demonstrate increased flow on color Doppler.[14] On CT orbital varices appear as avidly enhancing, dilated, and tortuous vessels, similar to varices in other parts of the body (Fig. 5). MRI typically demonstrates an enhancing retrobulbar mass with flow voids, although if they are thrombosed or have slow flow they may appear as soft tissue masses.[13] CT is preferred over MRI because CT can be performed with and without Valsalva maneuver to appreciate changes in the lesion configuration.[14]

Infantile Hemangiomas

Infantile hemangiomas (previously known as capillary hemangiomas) are the most common orbital tumors of infancy.[14] They usually involve the cutaneous portion of the eyelids and may have additional superficial or deep components.[15] They are almost always extraconal in location and can extend intracranially via the optic canal or superior orbital fissure.[15] On physical examination, superficial lesions appear red, whereas subcutaneous lesions appear blue.[16] They grow rapidly within the first 6 months of life then involute.[15] Imaging serves to delineate the extent of the mass and can reveal portions that are not visible clinically. Similar to hemangiomas in other parts of the body like the liver, capillary hemangiomas are hyperechoic on US.[16] On CT, capillary hemangiomas appear as lobulated, irregular lesions which demonstrate homogenous enhancement. On MRI, they are typically T1 hypointense and T2 isointense to mildly hyperintense and demonstrate avid

contrast enhancement. In contrast, venous malformations are very T2 hyperintense.

Cavernous Hemangioma

Cavernous hemangiomas by ISSVA classification are actually venous malformations therefore the appropriate term cavernous venous malformations. They are the most common orbital vascular lesions in adults and typically occur in middle-aged women.[17] They slowly enlarge over time and patients classically present with painless proptosis.[17] Unlike the capillary hemangiomas of infancy, cavernous hemangiomas do not involute. They are usually found in the intraconal space and rarely involve the orbital apex or extend intracranially. On histology, these lesions are composed of dilated vascular channels lined by a fibrous pseudocapsule. For this reason, these lesions appear as avidly enhancing well-circumscribed lesions on imaging. MRI is superior to CT in distinguishing cavernous hemangiomas from other vascular orbital lesions.[17] On MRI, they appear as T1 isointense and very T2 hyperintense (Figs. 6A, C). On T2-weighted imaging, there are often internal septations and a T2 hypointense rim corresponding to the fibrous pseudocapsule. On contrast-enhanced imaging, these lesions demonstrate heterogenous enhancement (Fig. 6B). If multiphase imaging is performed, it often demonstrates patchy heterogenous enhancement in the arterial phase with progressive central enhancement in the venous phase. CT findings resemble that of the MRI, with lesions appearing as well-defined high-attenuation masses that demonstrate heterogenous enhancement on single-phase imaging and progressive enhancement on multiphase imaging (Fig. 6D).

Venous Lymphatic Malformations

Venous lymphatic malformations are vascular malformations with slow flow and no flow components, and are the most common vascular orbital mass in children.[14] Patients usually present in infancy or childhood with painless proptosis, similar to cavernous hemangiomas. However unlike many of the other vascular orbital lesions, venous lymphatic malformations often undergo internal hemorrhage, either spontaneously or after minor trauma, resulting in acute proptosis.[14] These lesions are diffuse and multispatial, often involving the intraconal and extraconal compartments.[16] MRI is the imaging modality of choice with the signal characteristics varying depending on the protein concentration of the fluid in the cystic component as well as the age of the internal hemorrhage products. Typically, these lesions demonstrate T2 hyperintensity and variable T1 signal intensity (Fig. 7). If there has been recent hemorrhage, fluid-fluid levels are visible and are virtually pathognomonic for lymphatic malformations.[16] On US, they cystic lesions are poorly

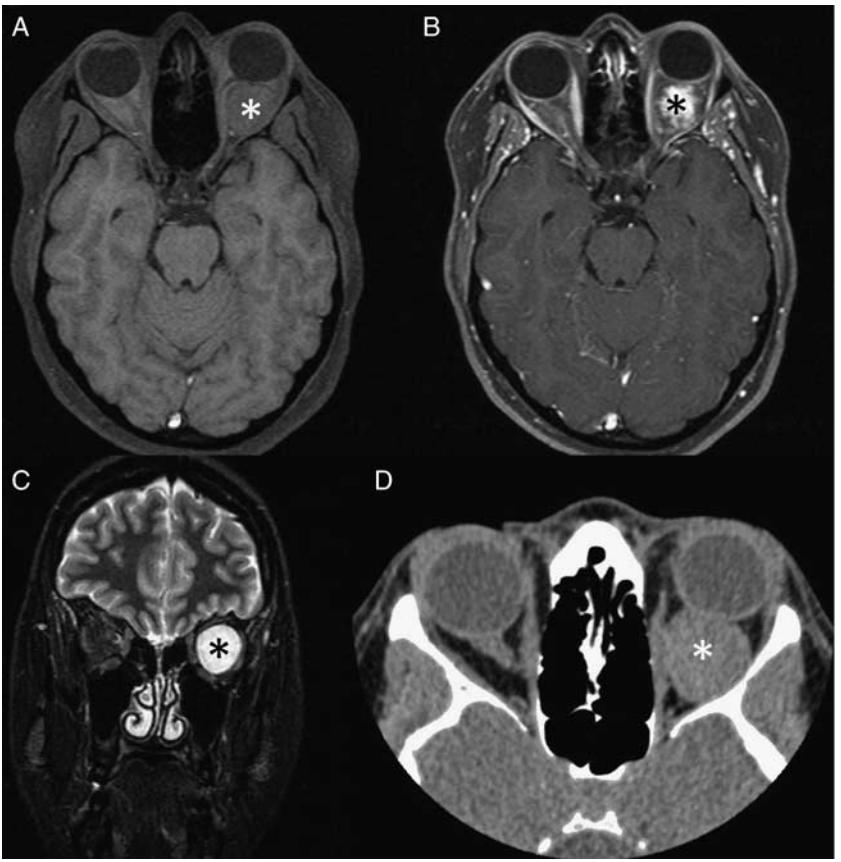

Figure 6. *42-year-old woman with longstanding proptosis was found to have a retrobulbar mass with imaging features consistent with a cavernous hemangioma. The patient was asymptomatic and elected to forego any surgical intervention. Axial T1-weighted fat-saturated noncontrast MRI demonstrates a well-circumscribed T1 isointense mass in the left intraconal space (A, white asterisk). Axial T1-weight fat-saturated postcontrast MRI demonstrates heterogenous enhancement of the mass (B, black asterisk). Axial T2-weighted MRI demonstrates a T1 hyperintense mass in the left intraconal space (C, black asterisk). Axial noncontrast computed tomography demonstrates a high-attenuation mass in the intraconal space (D, white asterisk). MRI indicates magnetic resonance imaging.*

defined and appear infiltrative. On CT, there are high-attenuation multicompartmental lesions with minimal enhancement. Phleboliths in the venous component of the lesion may be seen as focal calcifications.

Carotid Cavernous Fistula

CCFs represent an abnormal communication between the cavernous sinus and a branch of the internal carotid artery, external carotid artery or both. CCFs can be classified according to flow (high flow vs. low flow),

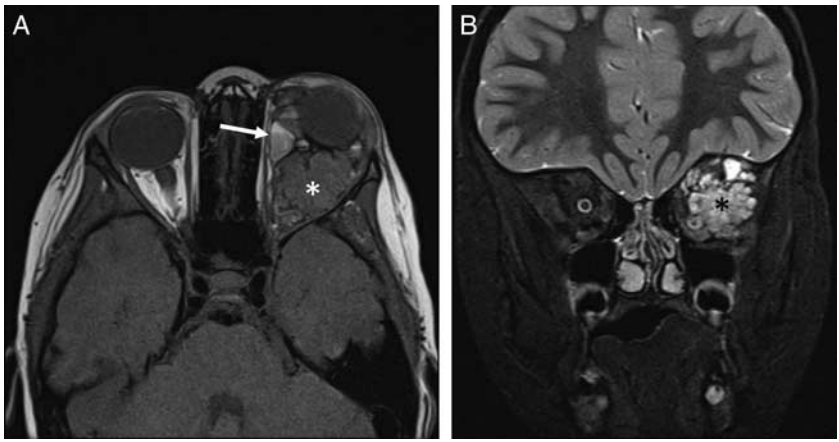

Figure 7. *2-year-old boy presented to ophthalmologist with 6 months of progressive proptosis and was found to have a venous lymphatic malformation. Axial T1-weighted noncontrast MRI (A) demonstrates a predominantly T1 isointense mass with fluid-fluid levels (white arrow) centered in the left intraconal space extending into the medial and superior extraconal spaces. This results in mild proptosis (white asterisk). Coronal T2-weighted MRI demonstrates a heterogenous T2 hyperintense multispatial retrobulbar mass (B, black asterisk). MRI indicates magnetic resonance imaging.*

etiology (trauma or spontaneous), or anatomy (direct or indirect).[18] CCFs are most commonly categorized based on their anatomy, as either direct (arterial supply arising directly from the ICA) or indirect (arterial supply from branch of internal carotid or external carotid artery). Another widely used anatomic classification of CCFs is the Barrow classification, originally described in 1985.[19] It divides CCFs into 4 subtypes according to their arterial supply: (A) main internal carotid artery; (B) dural branch of the internal carotid artery; (C) dural branch of the external carotid artery; or (D) dural branches of both the internal and external carotid arteries.[20] Type A is high flow, direct CCF that most commonly occurs secondary to trauma. Types B to D are slow flow, indirect lesions that occur in older women, often due to cavernous aneurysms, connective tissue disease, or venous sinus thrombosis.[18] The classic clinical trial is pulsatile exophthalmos, orbital bruit, and conjunctival congestion.[21] CT and MRI are the initial diagnostic imaging tests of choice but digital subtraction angiography is ultimately required to precisely classify the lesion. CT findings of CCFs include enlargement and tortuosity of the superior ophthalmic vein and enlargement of the ipsilateral cavernous sinus (Fig. 8). There is often enlargement of the extraocular muscles and ipsilateral proptosis. On MRI, findings are similar to CT with the addition of abnormal flow voids in the affected cavernous sinus. Catheter angiography can distinguish between the various subtypes, and is combined with catheter-based endovascular techniques when trying to close the fistula.

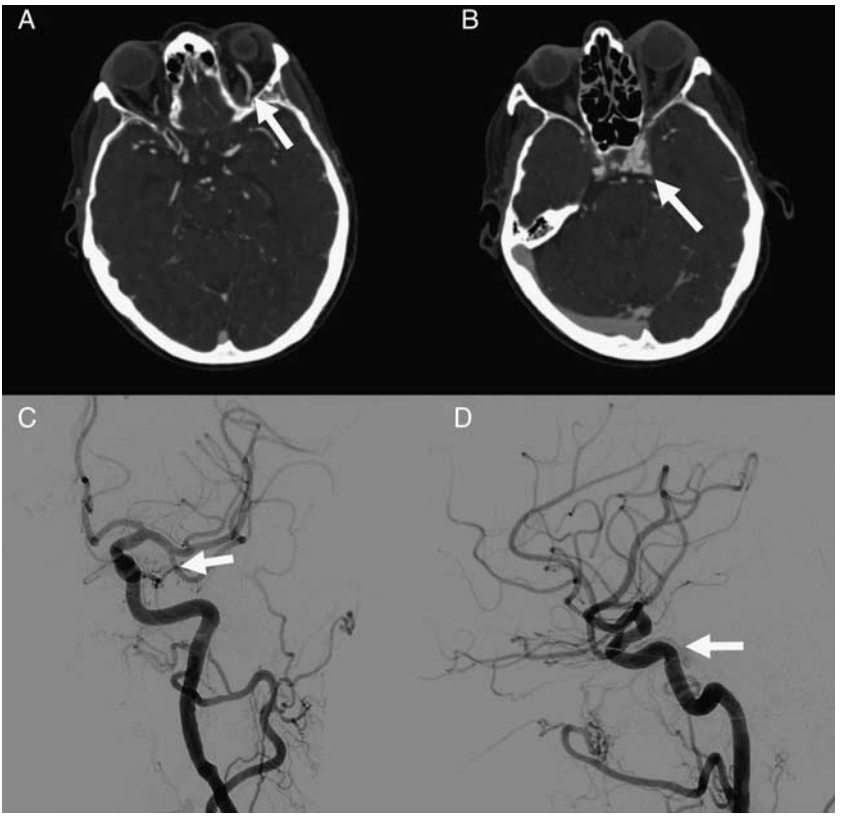

Figure 8. *84-year-old woman presented with progressive left chemosis, proptosis, and elevated intraocular pressure for 2 months. Axial CT angiogram through the orbits demonstrates hyperenhancement and dilation of the left superior ophthalmic vein (A, white arrow). CT angiogram in the same patient at the level of the cavernous sinus demonstrates hyperenhancement and enlargement of the left cavernous sinus (B, white arrow). Anteroposterior and lateral views of left internal carotid artery digital subtraction angiogram demonstrates abnormal filling of the ipsilateral venous sinus (C and D, white arrows). There was evidence of filling from the internal and external carotid arteries consistent with type D carotid cavernous fistula. CT indicates computed tomography.*

■ Orbital Tumors

A wide variety of inflammatory and neoplastic lesions can affect the orbital tissue and bony orbit. Although, histopathologic analysis is often required to confirm the diagnosis, in some cases the radiologic findings can often provide strong diagnostic considerations.

Dermoid and Epidermoid Cysts

Orbital dermoid and epidermoid cysts are common congenital masses thought to arise from entrapped ectoderm within the bony sutures of the

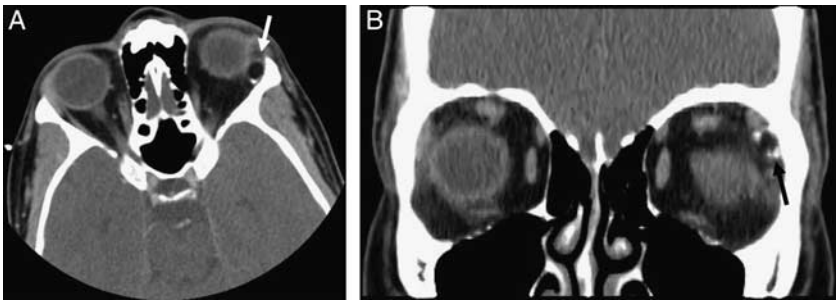

Figure 9. *43-year-old woman presented to ophthalmology clinic with 1 year of recurrent dacryoadenitis. Axial (A) and coronal (B) computed tomographic images through the orbit demonstrate a mass in the left lacrimal gland containing soft tissue, fat, and calcification (arrows).*

orbit.[14] They are not neoplasms but rather cysts lined by an ectodermal endothelium.[22] The primary difference between dermoids and epidermoids is that dermoids contain adnexal structures such as hair follicles and sebaceous glands.[23] These lesions typically present in the first decade of life as painless periorbital masses. They slowly enlarge over time and often produce indolent bony erosion and remodeling. On CT they appear as ovoid, well-defined cystic structures. The Hounsfield units of the cyst will depend on its contents. Dermoids will typically have negative attenuation values due to high lipid contents, whereas epidermoids typically have a density resembling cerebrospinal fluid (CSF) (Fig. 9). On MRI, dermoids demonstrate signal characteristics similar to fat due to the high lipid content from sebaceous secretions. They are T1 hyperintense and lose signal on fat-suppressed images. If recently ruptured, there will be adjacent inflammatory changes. Epidermoid cysts demonstrate signal characteristics resembling CSF, which is T1 hypointense and T2 hyperintense. They can be distinguished from arachnoid cysts and CSF spaces with DWI (epidermoid cysts will demonstrate increased signal on DWI due to a combination of restricted diffusion and T2 shine through).[22]

Teratoma

Orbital teratomas are rare congenital cystic masses with ~70 cases reported in the literature.[24] Histologically they contain all 3 (ectoderm, mesoderm, and endoderm) embryonic germ cell layers.[25] Patients classically present at birth with severe unilateral proptosis.[26] These lesions grow rapidly over time if untreated, due to mucus secretion from the embryonic intestinal tissue.[24] CT shows a multiloculated cystic mass with areas of fat attenuation, calcification, and ossification. On MRI, there is variable signal intensity on T1 and T2-weighted imaging, related to the different contents of the cyst. For instance, areas with high lipid content will demonstrate T1 hyperintensity. Teratomas can be distinguished from other T1 hyperintense lesions such as hemorrhagic cysts with the

use of fat suppression techniques or the presence of chemical shift artifact.

Rhabdomyosarcoma

Rhabdomyosarcoma is the most common pediatric extraocular orbital malignancy.[22] It classically presents with rapidly progressive proptosis in children with a peak age of 8 to 9 years.[14] They commonly arise in the superior aspect of the orbit and may erode adjacent bone and extend intracranially. These masses have an imaging appearance resembling other sarcomas. US demonstrates a heterogenous mass that is isoechoic to hypoechoic in echogenicity with variable flow on color Doppler.[27] CT shows an enhancing soft tissue mass that is isoattenuating relative to the extraocular muscles. In later stages of the disease, the mass may appear more heterogenous due to hemorrhage or necrosis and there may be invasion of the bony orbit.[27] On MRI, these lesions are T1 isointense and T2 mildly hyperintense to hypointense with homogenous enhancement (Fig. 10).[28]

Lymphoma

Orbital lymphoma is the most common primary orbital tumor in older adults.[29] Most orbital lymphomas are low-grade non-Hodgkin lymphomas, with marginal zone B-cell lymphoma of the mucosa-associated lymphoid tissue being the most common subtype.[30] While only 1% of patients with systemic non-Hodgkin lymphomas have orbital involvement, ~75% of patients with orbital lymphoma will have systemic involvement.[31] Patients typically present with some combination of painless proptosis, diplopia,

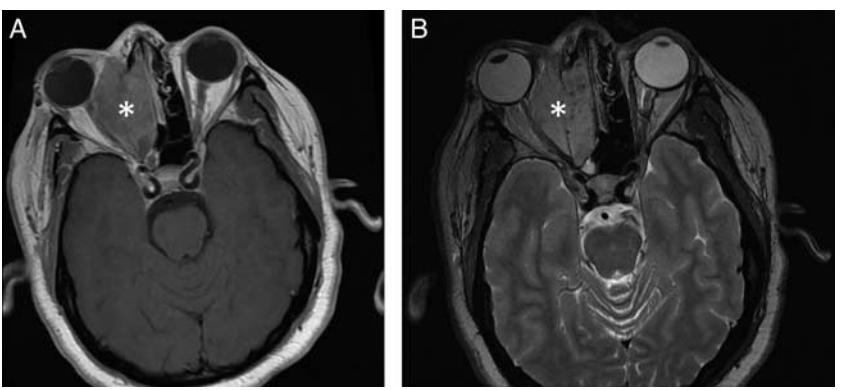

Figure 10. *46-year-old woman was initially treated with antibiotics for presumed sinusitis. She underwent an MRI after acute right monocular vision loss and was found to have a right alveolar rhabdomyosarcoma. Axial T1-weighted noncontrast MRI demonstrates a T1 isointense mass involving the right ethmoid sinus and extraconal orbit extending into the orbital apex (A, white asterisk). Axial T2-weighted MRI demonstrates this mass to be T2 hyperintense (B, white asterisk). MRI indicates magnetic resonance imaging.*

and restricted eye movements.[32] Although, they can occur anywhere in the orbit the most frequent sites of involvement include the lacrimal gland, conjunctiva, and eyelid.[31] CT shows an irregular, poorly defined mass that demonstrates contrast enhancement with no bony erosion (Fig. 11A).[33] MRI demonstrates a lesion that is T1 isointense and T2 hypointense.[34] On DWI, a distinguishing feature of orbital lymphomas is restricted diffusion because of their high histopathologic cellularity (Figs. 11C, D).[35]

Metastasis Both Soft Tissue and Bone Orbital metastases are rare and typically only encountered in older patients with widespread metastatic disease. The prevalence of orbital metastases in cancer patients

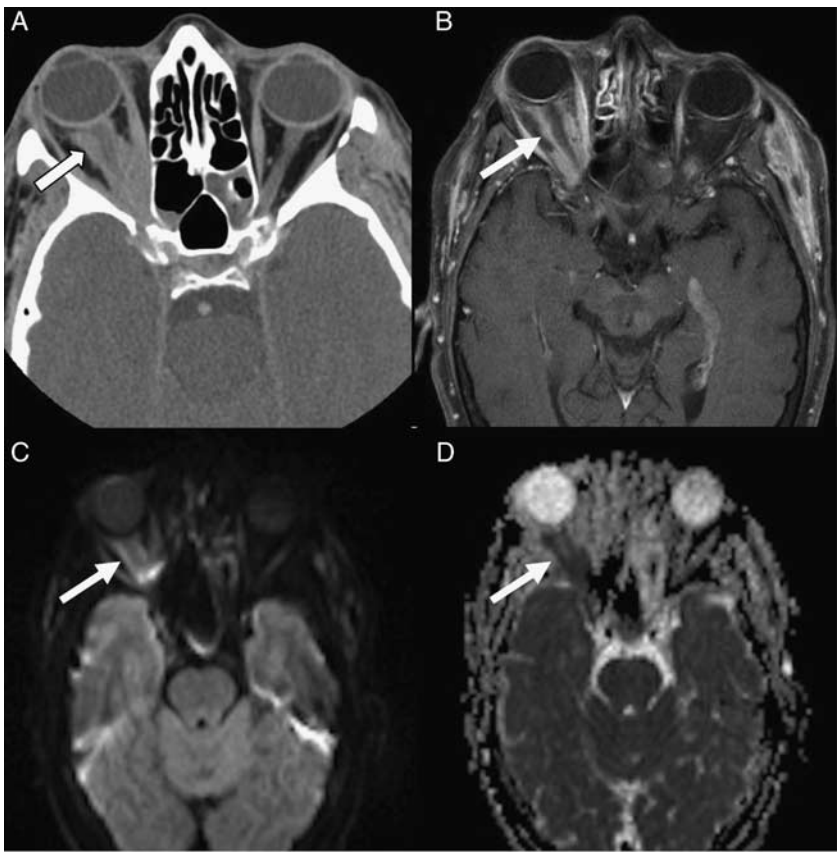

Figure 11. *68-year-old woman with a history of marginal zone lymphoma presented with progressive right eye proptosis. Axial contrast-enhanced computed tomography demonstrates enhancing soft tissue extending from the orbital apex in the intraconal space along the optic nerve (A, white arrow). Axial T1-weighted postcontrast fat-saturated magnetic resonance imaging demonstrates the same infiltative intraconal hyperenhancing mass (B, white arrow). The mass demonstrates high signal on diffusion weighted imaging (C, white arrow) and low signal on apparent diffusion coefficient (D, white arrow), consistent with restricted diffusion and characteristic of lymphoma.*

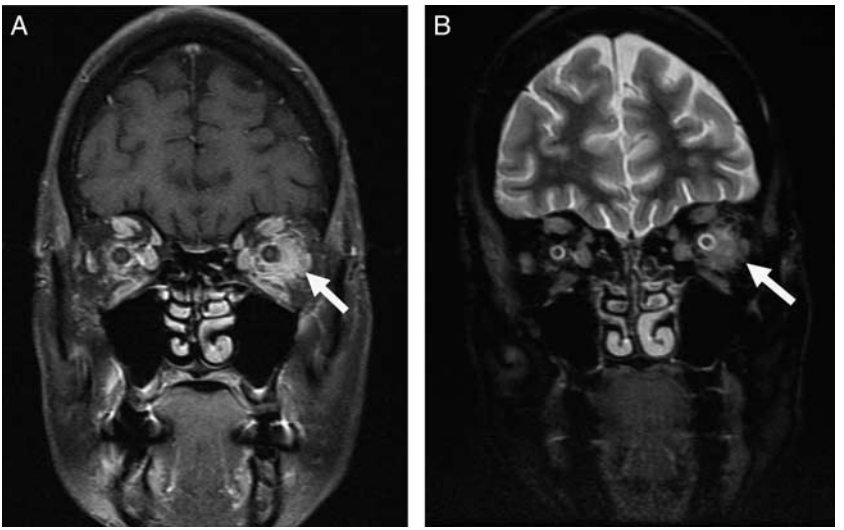

Figure 12. *64-year-old woman with metastatic breast cancer developed headaches and diplopia. MRI demonstrates breast cancer metastases to the orbits. Coronal T1-weighted fat saturation postcontrast MRI demonstrates irregular enhancing intraconal soft tissue as well as abnormal enhancement of the bilateral optic nerves (A, white arrow). Coronal T2-weighted MRI demonstrates T2 hyperintensity surrounding the left greater than right optic nerves (B, white arrow). MRI indicates magnetic resonance imaging.*

is estimated to range from 2% to 5%.[36] The most common associated malignancies are carcinomas from breast, lung, or prostate.[36] Symptoms are related to mass effect from the tumor and may include proptosis, diplopia, and pain. Scirrhous adenocarcinoma orbital metastases most often arise from the breast and characteristically produce enophthalmos.[36] Imaging findings can range from a discrete mass to diffusely infiltrating lesion that may be intraconal or extraconal in location. Prostate cancer classically metastasizes to bone, whereas breast cancer and melanoma metastasize to the orbital fat and extraocular muscles.[37] MRI findings depend on the type of underlying cancer but typically show heterogenous T1 hypointense and T2 isointense to hyperintense signal with diffuse enhancement of the involved structures (Fig. 12).[34]

Neurofibroma

Neurofibromas are benign nerve sheath tumors of the peripheral nervous system, classified as either localized, diffuse, or plexiform. The plexiform type is most commonly associated with neurofibromatosis (NF) type I while the localized type commonly occurs spontaneously.[38] Patients present with progressive proptosis and eventually diplopia depending on the size of the mass. If there is compression of the optic nerve, which most commonly occurs with orbital apex lesions, visual changes can occur.[38] On

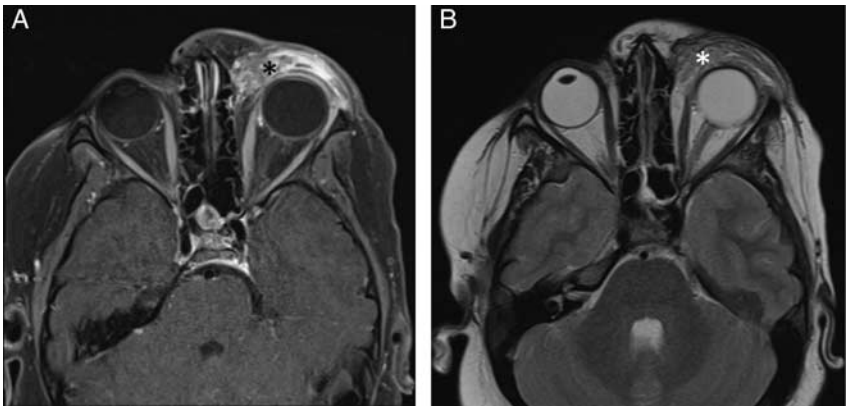

Figure 13. *8-year-old boy presented with left eyelid swelling and ptosis, and was found to have a left orbital plexiform neurofibroma. Genetic testing for neurofibromatosis I was negative. Axial T1-weighted postcontrast fat-saturated MRI demonstrates a heterogenously enhancing transpatial mass in the preseptal soft tissues (A, black asterisk). Axial T2-weighted MRI demonstrates the mass to be heterogenously T2 hyperintense; the classic "target" is not well visualized (B, white asterisk). MRI indicates magnetic resonance imaging.*

CT, these tumors are low in attenuation with minimal to no contrast enhancement. On MRI, they are T1 hypointense and T2 hyperintense with heterogenous enhancement (Fig. 13). Plexiform neurofibromas classically demonstrate the "target sign," which is the T2 hypointense fibrocollagenous core surrounded by T2 hyperintense myxomatous rim.[39]

Fibrous Dysplasia

Fibrous dysplasia is a benign congenital disease in which normal bone is replaced by fibro-osseous tissue.[40] Fibrous dysplasia is frequently discovered incidentally during childhood or adolescence. In ~75% of cases the disease affects 1 bone (monostotic) but it can affect multiple bones (polyostotic).[41] Craniofacial bony involvement occurs in 25% of monostotic and 50% of polyostotic cases.[41] The most common skull lesions involve the frontal, sphenoid, maxillary, and ethmoid bones.[42] On CT, fibrous dysplasia is easily diagnosed appearing as an expansile ground glass lesion (Fig. 14).[43] In contrast, fibrous dysplasia is more difficult to recognize on MRI and can be mistaken for malignant tumor. Lesions are typically T1 isointense and T2 hypointense with heterogenous enhancement.[42,43]

Orbital Pseudotumor and Tolosa Hunt Syndrome

Orbital pseudotumor, also known as idiopathic orbital inflammatory syndrome, is the second most common cause of exophthalmos.[44] Patients present with acute, painful, unilateral proptosis often associated with diplopia. The most common site of disease is in the extraocular muscles (ie, orbital

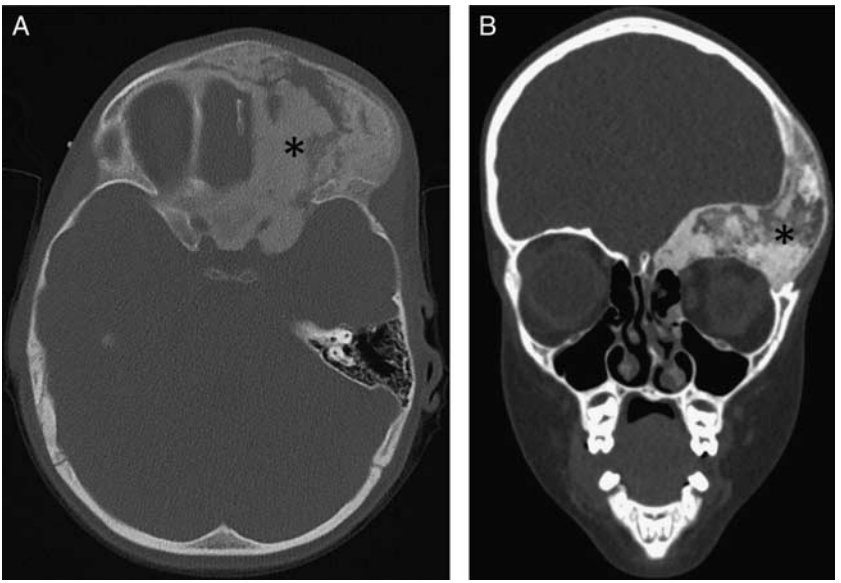

Figure 14. *3-year-old boy failed his vision screening test and was noted to have a bony protuberance around the left orbit. Axial (A) and coronal (B) noncontrast computed tomographic images demonstrates an expansile ground glass osseous mass involving the left superior orbital rim, left frontal calvarium, left sphenoid and anterior skull base consistent with fibrous dysplasia (black asterisks). This resulted in narrowing of the optic canal and superior orbital fissure accounting for his visual deficits (not shown).*

myositis). The typical imaging findings include enlargement of ≥1 extraocular muscles with involvement of the muscle belly. Tendinous involvement differentiates orbital myositis from its counterpart thyroid-associated orbitopathy. There may be additional inflammation involving the adjacent intraorbital fat and lacrimal gland. On MRI, the affected region is typically T1 and T2 isointense to hypointense with diffuse enhancement (Fig. 15).

Tolosa Hunt syndrome is a subtype of orbital pseudotumor that involves the orbital apex and cavernous sinus. It can affect patients of any age with no sex predilection. It classically presents with acute onset of unilateral painful ophthalmoplegia due to oculomotor nerve involvement in the cavernous sinus, although occasionally other cranial nerves may be affected.[45] MRI is the primary diagnostic imaging modality and demonstrates enhancing T1 isointense, T2 isointense soft tissue in the cavernous sinus possibly extending to the orbital apex (Fig. 16).[46] CT has a limited role in the diagnostic evaluation because of its poor sensitivity to detect the inflammation.[46]

Thyroid-associated Orbitopathy

Thyroid-associated orbitopathy, also known as Graves ophthalmopathy, is the most common cause of exophthalmos.[44] Patients typically present with proptosis as well as edema and erythema of the periorbital soft tissues and

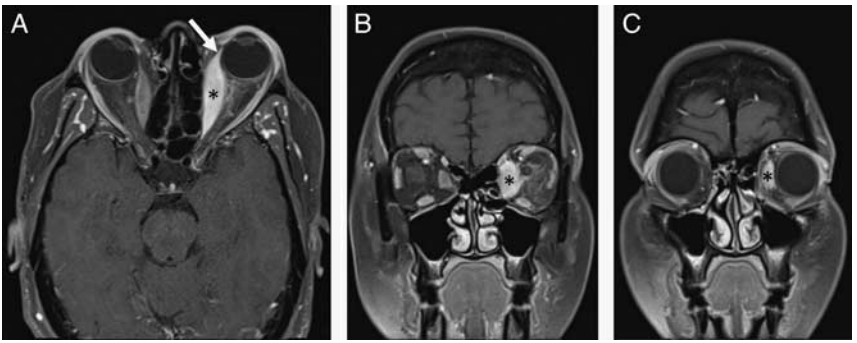

Figure 15. *45-year-old woman presented with left eye pain and diplopia for 3 weeks and subsequently underwent biopsy of the medial rectus demonstrating pseudotumor. Axial (A) and coronal (B, C) T1-weighted postcontrast fat-saturated magnetic resonance imaging demonstrates abnormal thickening and enhancement of the left medial rectus (black asterisks) with involvement of the myotendinous junction (white arrow) and stranding within the intraconal fat. Involvement of the myotendinous junction can be subtle as in this case and comparison with the normal right side is helpful for identification.*

conjunctivae.[47] It is usually painless, although a small proportion of patients with severe disease experience pain.[47] On CT, there is bilateral extraocular muscle enlargement with sparing of the tendinous insertions. The inferior rectus is most frequently involved, followed by the medial rectus, superior rectus, lateral rectus, and the superior and inferior oblique muscles. MRI findings include T2 hyperintensity and enhancement of the affected tissues (Fig. 17).

Intraorbital Optic Nerve Sheath Complex Lesions

Optic Pathway Gliomas Most optic pathway gliomas occur in children and are classified as World Health Organization grade I pilocytic

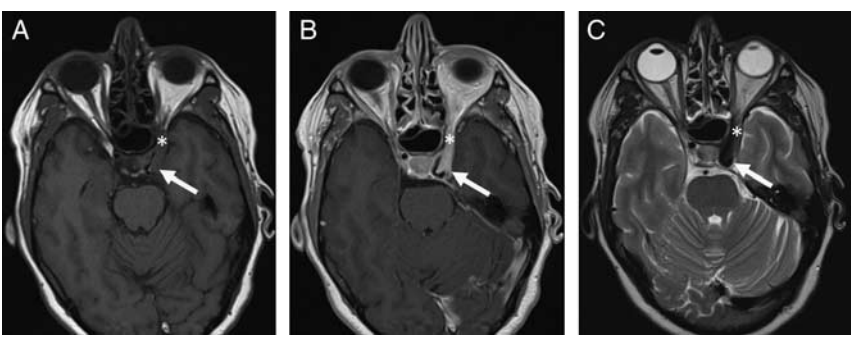

Figure 16. *45-year-old woman presented with left eye pain and diploplia and subsequently improved after a 6-week course of steroids. Magnetic resonance imaging findings are consistent with Tolosa Hunt syndrome. Axial T1-weighted precontrast (A), postcontrast (B), and T2-weighted imaging (C) demonstrates enhancing T1 isointense, T2 hypointense enlargement of the left cavernous sinus (white arrows) extending to the orbital apex (white asterisks).*

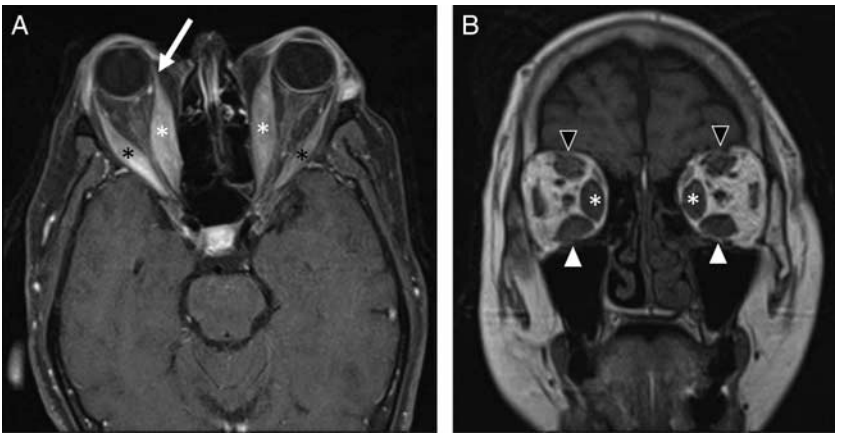

Figure 17. *59-year-old woman with a history of Graves disease presented to the emergency department with acute onset of bilateral eye swelling and diplopia. Axial (A) T1-weighted postcontrast fat-saturated MRI demonstrates abnormal thickening and enhancement of the right greater than left medial (white asterisks) and lateral rectus muscles (black asterisks) with sparing of the tendinous insertion (white arrow). Coronal (B) T2-weighted shows enlargements of the bilateral superior rectus (black arrow heads), medial rectus (white asterisks), and inferior rectus muscles (white arrow heads).*

astrocytomas. They usually involve the optic nerve but can arise anywhere along the optic pathway. It has been estimated that 10% to 70% of children with an optic pathway glioma have NF I. Approximately 6% to 20% of NF I patients have an optic pathway glioma.[48,49] Symptoms vary depending on the location of the tumor. For those lesions occurring along the optic nerve, symptoms include proptosis, visual field deficits, optic nerve atrophy, and strabismus.[49] If the tumor affects the hypothalamus, endocrine disorders such as growth hormone deficiency or precocious puberty can occur.[50] Imaging findings at CT include enlargement and kinking of the optic nerve.[51] MRI demonstrates a T1 isointense, heterogenously T2 hyperintense lesion with variable enhancement (Fig. 18).[51] Higher grade gliomas, such as World Health Organization grade IV glioblastoma, can occur along the optic pathways but are very rare and typically present in older adults.

Optic Nerve Sheath Meningioma Meningiomas are extremely common tumors of the dura, but only 1% of meningiomas involve the optic nerve sheath.[52] Optic nerve sheath meningiomas account for an estimated 5% to 10% of orbital tumors.[53] They most commonly occur in middle-aged women who present with the classic triad of visual loss, optic atrophy, and optociliary shunt vessels.[54] On CT and MRI, these tumors usually appear as diffuse thickening of the optic nerve sheath (Fig. 19).[54] The tumor will enhance around the nonenhancing optic nerve, producing the classic "tram-track" sign.[55] Internal calcification, while variably present and often only visible on CT, favors a meningioma over other neoplasms that occur in this location such as optic pathway gliomas.

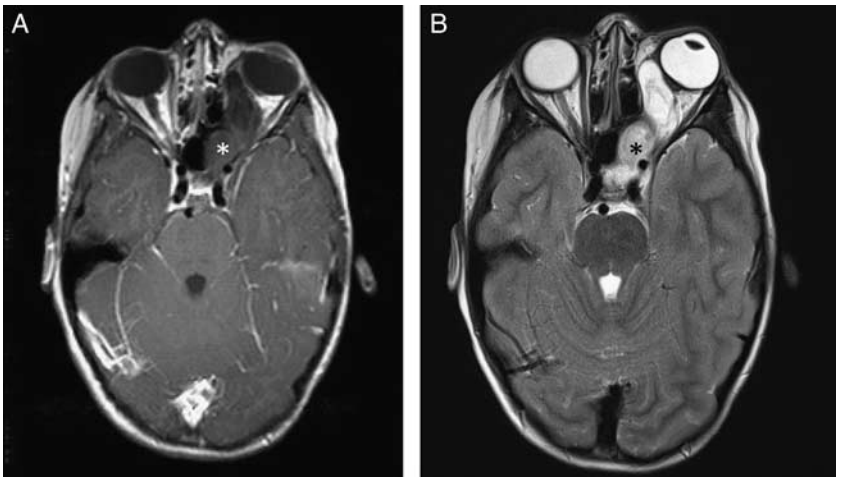

Figure 18. *9-year-old girl was diagnosed with an optic glioma (pilocytic astrocytoma) after she was noted to have a left gaze preference. Genetic testing for neurofibromatosis I was negative. Axial T1-weighted postcontrast fat-saturated MRI demonstrates an isointense peripherally enhancing mass extending from the posterior optic chiasm into the left optic nerve and medial left orbit (A, white asterisk). Axial T2-weighted MRI demonstrates the mass to be heterogenously T2 hyperintense (B, black asterisk). MRI indicates magnetic resonance imaging.*

Optic Neuritis

Optic neuritis is inflammation of the optic nerve due to any cause but most commonly encountered in demyelinating diseases such as multiple sclerosis (MS) and neuromyelitis optica (NMO).[56] In the setting of MS, it

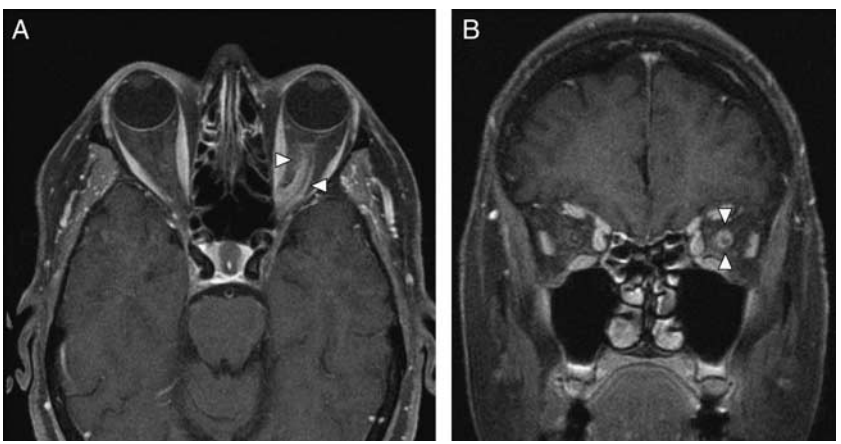

Figure 19. *75-year-old woman presented to her ophthalmologist with a left visual field cut and was found to have an optic nerve sheath meningioma. Axial (A) and coronal (B) T1-weighted postcontrast fat-saturated magnetic resonance imaging demonstrates diffuse thickening and enhancement of the left optic nerve sheath with relative sparing of the optic nerve (white arrow heads).*

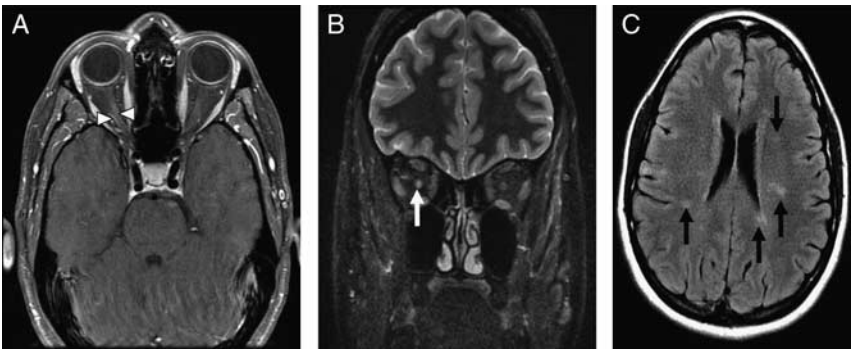

Figure 20. *37-year-old woman developed painful right eye movement and was found to have an afferent pupillary defect and optic nerve edema on examination. Axial T1-weighted postcontrast fat-saturated MRI demonstrates asymmetric enhancement and enlargement of the right optic nerve (A, white arrow heads). Coronal T2-weighted MRI demonstrates abnormally increased T2 hyperintensity within the right optic nerve (B, white arrow). Axial FLAIR MRI demonstrates periventricular T2 hyperintense lesions oriented perpendicular to the lateral ventricles consistent with multiple sclerosis (C, black arrows). FLAIR indicates fluid attenuation inversion recovery; MRI, magnetic resonance imaging.*

typically occurs in young adult females presenting as painful unilateral vision loss. Patients with NMO are typically older than MS patients and present with bilateral optic neuritis and longitudinally extensive transverse myelitis.[57] CT has a limited role in the diagnosis of optic neuritis and is usually unremarkable. MRI is the imaging modality of choice and findings typically include an enlarged, hyperenhancing, T2 hyperintense optic nerve (Figs. 20, 21).[44]

Lacrimal Gland Abnormalities

Pleomorphic Adenoma Pleomorphic adenoma, also known as benign mixed tumor, is the most common tumor of the lacrimal gland that classically presents as a slow painless swelling of the upper lid in the fourth or fifth decade of life.[58,59] CT demonstrates a well-defined, enhancing lacrimal fossa soft tissue mass, which may result in adjacent bony remodeling without bony destruction (Fig. 22).[58] MRI findings include a homogenously enhancing T1 hypointense, T2 hyperintense lacrimal gland mass.[34]

Adenoid Cystic Carcinoma Adenoid cystic carcinoma is the most common lacrimal gland malignancy accounting for ~5% of all primary orbital neoplasms.[59] It classically presents during the fourth decade of life with symptoms of globe dystopia, proptosis, and "S"-shaped ptosis.[60] Perineural spread is common and typically painful.[34] Adenoid cystic carcinoma can resemble pleomorphic adenoma. However, findings

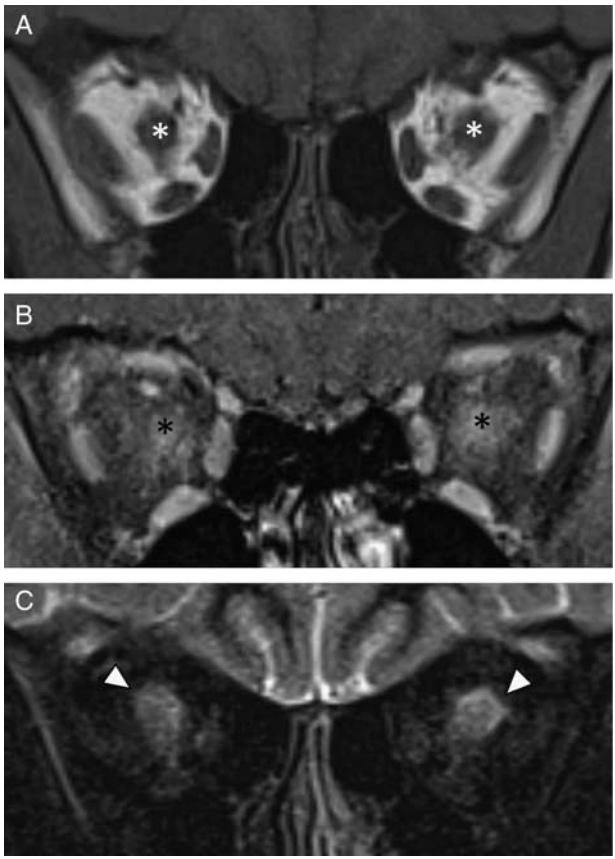

Figure 21. *49-year-old woman presented with acute onset of bilateral ocular pain and visual disturbances. Laboratory tests were positive for aquaporin-4 autoantibody, consistent with neuromyelitis optica. Axial (A) T1-weighted precontrast MRI shows enlargement of the bilateral optic nerves (white asterisks). Coronal (B) T1-weighted postcontrast fat-saturated MRI demonstrates abnormal enhancement within the bilateral optic nerves (black asterisks). Coronal (C) T2-weighted MRI shows abnormal T2 hyperintense signal in the bilateral optic nerves (white arrow heads). MRI indicates magnetic resonance imaging.*

suggestive of carcinoma include infiltrative and irregular borders with bony erosion and areas of calcification (Fig. 23).[34] Recently, DWI was shown to be helpful in distinguishing benign from malignant lacrimal gland lesions, with malignant lesions demonstrating lower apparent diffusion coefficient values (Fig. 23).[61]

Mucoepidermoid Carcinoma Mucoepidermoid carcinoma is the most common malignant tumor of the salivary gland but rarely occurs in the lacrimal gland, accounting for only 2% of all malignant lacrimal gland tumors.[62] Patients typically present in the fifth decade of life with a painless mass in the superotemporal orbit with proptosis, diplopia,

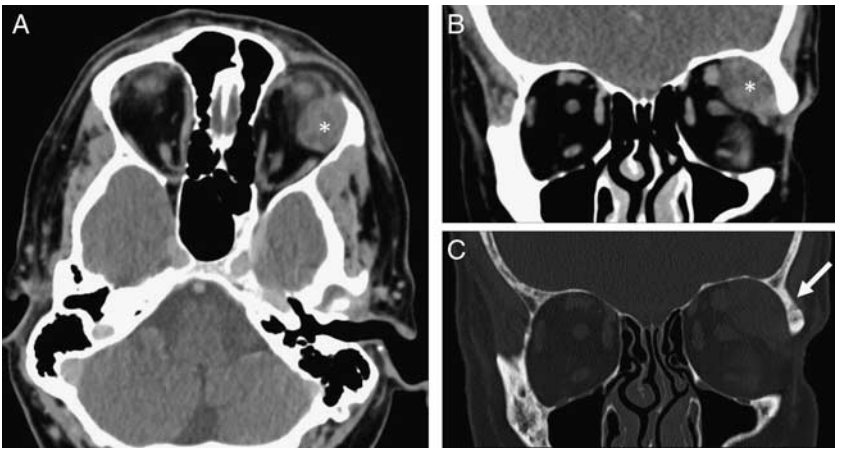

Figure 22. *61-year-old man presented with painless left eye fullness and was found to have 4 mm of proptosis on examination. Axial (A) and coronal (B) contrast-enhanced computed tomographic images demonstrate an enhancing soft tissue mass in the left lacrimal gland (white asterisk). Coronal computed tomographic image (C) viewed in bone window settings demonstrates bony thickening and sclerosis of the left lateral orbital wall adjacent to the mass (white arrow).*

and impaired extraocular muscle movement.[63] CT and MRI findings resemble other malignant lacrimal gland lesions like adenoid cystic carcinoma including an irregular, infiltrative mass with bony invasion and calcification.[63,64]

Lymphoma Lymphoma of the lacrimal gland is relatively uncommon, accounting for ~7% to 25% of orbital lymphomas.[65] However, they

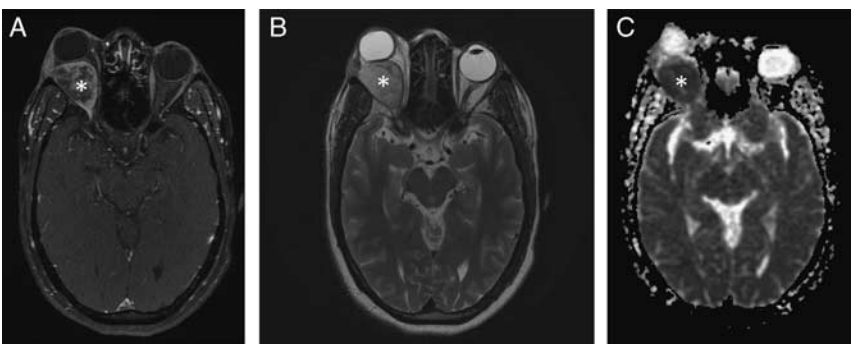

Figure 23. *43-year-old man presented with subacute right eye proptosis and underwent resection of a right lacrimal gland mass, which was demonstrated to be adenoid cystic carcinoma at pathology. Axial T1-weighted postcontrast fat-saturated MRI demonstrates an enhancing right retrobulbar orbital mass involving the extraconal and intraconal spaces and extending to the orbital apex (A, white asterisk). Axial T2-weighted MRI demonstrates the mass to be heterogenously T2 hyperintense (B, white asterisk). Axial apparent diffusion coefficient MRI shows the mass is hypointense consistent with restricted diffusion (C, white asterisk). MRI indicates magnetic resonance imaging.*

account for up to 37% of all malignant lacrimal gland lesions.[65] They arise in older women and may be limited to the orbit alone or be part of a systemic lymphoma.[59] Symptoms include a painless mass in the upper outer orbit that may result in local mass effect depending on the size. The most common subtype of lymphoma in the lacrimal gland is marginal zone lymphoma.[65] CT and MRI findings of lacrimal gland lymphoma are identical to that of ocular adnexal lymphoma involving other parts of the orbit.[66] CT and MRI demonstrates a soft tissue mass in the lacrimal gland that homogenously enhances and restricts diffusion.[66] It is typically T1 isointense to hyperintense and T2 isointense.[66]

Sarcoidosis Sarcoidosis is a systemic granulomatous inflammatory process that affects the orbit in up to 80% of patients.[67] Sarcoid can affect any part of the orbit including the conjunctiva, retrobulbar space, muscles, lacrimal glands, globe, or optic nerves.[68] Lacrimal gland involvement is rare, occurring in <2% of sarcoidosis cases.[69] The most common imaging findings include hyperenhancement and smooth enlargement of the lacrimal glands (Fig. 24).[70] Although lacrimal gland involvement by sarcoidosis may by unilateral, diffuse enlargement of the bilateral lacrimal glands is highly suggestive of sarcoidosis.[70] DWI can be used to distinguish lacrimal gland sarcoidosis that demonstrate restricted diffusion from lymphoproliferative lesions such as lymphoma.[35]

Granulomatous Polyangitis (GPA) GPA is a granulomatous autoimmune vasculitis that classically involves the renal and respiratory

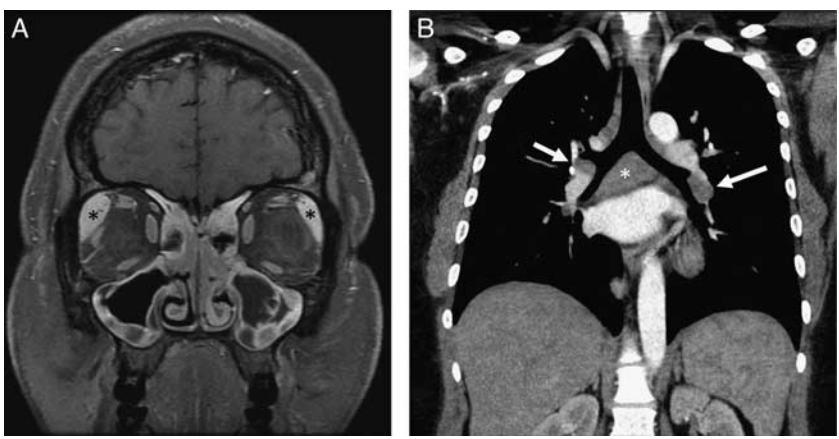

Figure 24. *29-year-old African American female was referred to ophthalmology for right eye redness and ultimately underwent right lacrimal gland biopsy demonstrating sarcoid. Coronal T1-weighted postcontrast fat-saturated magnetic resonance imaging demonstrates hyperenhancing, enlarged bilateral lacrimal glands (A, black asterisks). Coronal contrast-enhanced computed tomography demonstrates hilar (white arrows) and mediastinal (white asterisk) lymphadenopathy suggestive of sarcoid (B).*

systems. Orbital involvement occurs in up to 60% of patients and may be the presenting feature in up to 16% of cases.[71] Lacrimal gland involvement by GPA is rare and typically occurs in younger patients with a median age of 30 years.[71] Unlike sarcoid, lacrimal gland GPA is usually unilateral. Presenting symptoms are often related to sinonasal disease (eg, sinusitis and epistaxis).[72] CT and MRI findings typically include nasal septum destruction and findings of chronic sinusitis such as mucosal thickening, polypopsis, and osseous sclerosis.[73] There is typically unilateral enlargement of the lacrimal gland due to a homogenously enhancing soft tissue mass.[73]

Sjogren Syndrome Sjogren syndrome is a systemic autoimmune inflammatory disorder affecting the salivary and lacrimal glands resulting in xerostomia and keratoconjunctivitis sicca. It typically affects women in their 40s or 50s.[74] The imaging features resemble other inflammatory and lymphoproliferative conditions of the lacrimal gland.[58] CT demonstrates bilateral lacrimal gland enlargement.[75] MRI shows bilateral lacrimal gland enlargement that is T1 and T2 isointense.[58] It has also been shown to restrict diffusion.[76] It is important to note that patients with Sjogren syndrome are at an increased of lymphoma and there are no imaging features to reliably distinguish between the lymphoproliferative disease of Sjogren from that of malignant lymphoma.[75]

Orbital Pseudotumor The lacrimal gland is one of the most common sites of orbital pseudotumor.[77] Orbital inflammatory pseudotumor involving the lacrimal gland, also known as idiopathic dacryoadenitis, typically presents in the fifth decade of life,has a slight female predominance and typically unilateral.[78] Clinical symptoms include pain, upper eyelid swelling, proptosis, and impaired extraocular muscle function.[77] CT and MRI will demonstrate an enlarged, hyperenhancing lacrimal gland (Fig. 25). The inflammatory changes may extend outside the lacrimal gland and affect the orbital fat or adjacent extraocular muscles.[78]

■ Orbital Infections

Orbital infections are classified according to their location relative to the orbital septum. The orbital septum is the anatomic boundary between the eyelid and orbit and consists of a band of connective tissue extending from the periosteum of the orbital rim to the tarsal plate of the eyelid.[79]

Preseptal Cellulitis

Preseptal cellulitis, also known as periorbital cellulitis, is an infection of the soft tissues anterior to the orbital septum. Patients present with pain, erythema, and swelling of a unilateral eyelid but usually without

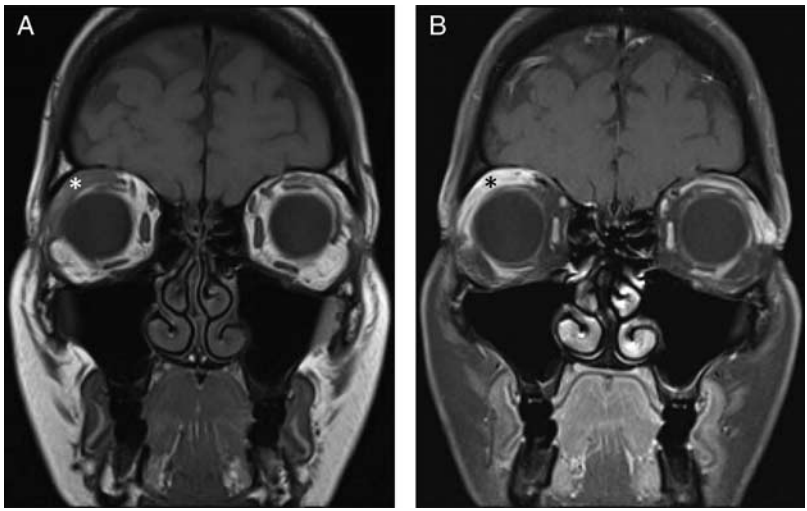

Figure 25. *8-year-old girl underwent an MRI for right eye ptosis and was found to have lacrimal gland pseudotumor on biopsy. Coronal T1-weighted noncontrast MRI demonstrates a T1 hypointense mass within the right lacrimal gland (A, white aterisk). Coronal T1-weighted postcontrast fat-saturated MRI demonstrates an enlarged, hyperenhancing right lacrimal gland (B, black asterisk). MRI indicates magnetic resonance imaging.*

proptosis or impaired eye movement.[80] CT is the imaging test of choice and helps to distinguish preseptal from postseptal cellulitis. CT demonstrates inflammation within the skin and subcutaneous tissues of the eyelid anterior to the orbital septum (Fig. 26). MRI will show T1 isointense and T2 hyperintense soft tissue thickening.[81]

Figure 26. *54-year-old woman presented to the emergency department with acute onset of left facial redness and swelling and was found to have preseptal cellulitis. Axial noncontrast computed tomography shows soft tissue thickening of the left preseptal soft tissues with no involvement of the postseptal tissues (white arrow).*

Postseptal Cellulitis

Postseptal cellulitis, also known as orbital cellulitis, is an infection that occurs within the orbit posterior to the orbital septum. It can be categorized according to involvement of the intraconal, extraconal, or subperiosteal compartments.[82] It is usually a complication of paranasal sinusitis but may be posttraumatic or postsurgical in etiology. Postseptal cellulisits initially manifests as inflammation and edema within the soft tissues that may then progress to phlegmonous changes and ultimately abscess formation.[81] CT will initially demonstrate enhancing, inflammatory changes in the postseptal soft tissues that may subsequently evolve into a rim-enhancing fluid collection if an abscess forms. MRI will demonstrate T1 hypointense, T2 hyperintense changes in the soft tissues reflecting edema and inflammation (Fig. 27). Important complications to recognize include cavernous sinus thrombosis and intracranial abscess formation.[82]

Subperiosteal Abscess

Subperiosteal abscess is a postseptal infection that consists of a collection of pus between the periorbita and involved sinus, most commonly occurring along the lamina papyracea.[81] It typically occurs in young adults as a complication of acute ethmoid sinusitis.[82] If large, the abscess can have local mass effect and result in displacement of the orbit causing proptosis. Vision is usually spared.[83] On CT, subperiosteal abscess presents as a rim-enhancing low density extraconal collection

Figure 27. *52-year-old woman presented to the emergency department with 2 weeks of left eye redness and swelling that was unresponsive to antibiotics. Axial T1-weighted postcontrast fat-saturated MRI (A) demonstrates thick, enhancing preseptal soft tissue (white arrow) extending posteriorly into the postseptal soft tissues (black arrow). There are areas of T1 hypointensity centrally, consistent with a multiloculated abscess (white asterisk). Axial T2-weighted MRI (B) demonstrates T2 hyperintense soft tissue thickening of the preseptal (white arrow) and postseptal (black arrow) soft tissues. MRI indicates magnetic resonance imaging.*

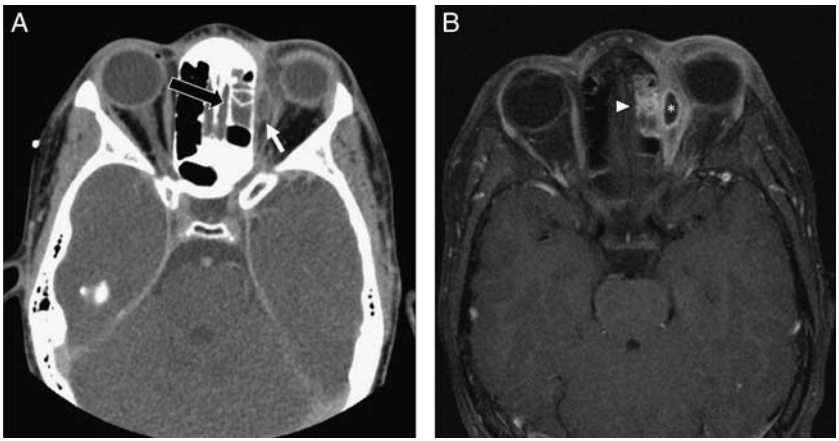

Figure 28. *10-year-old boy presented to the emergency department with 1 week of left eye erythema and edema. Axial contrast-enhanced computed tomography (A) shows a rim-enhancing low attenuation collection along the left lamina papyracea (white arrow). There is opacifcation of the underlying ethmoid air cells suggestive of sinusitis (black arrow). Axial T1-weighted postcontrast fat-saturated magnetic resonance imaging (B) demonstrates the subperiosteal abscess along the left lamina papyracea (white asterisk) with underlying ethmoid sinusitis (white arrow head).*

along the bone adjacent to a sinus, typically with underlying signs of sinusitis (Fig. 28). MRI will show a rim-enhancing fluid collection that demonstrates restricted diffusion (Fig. 28).

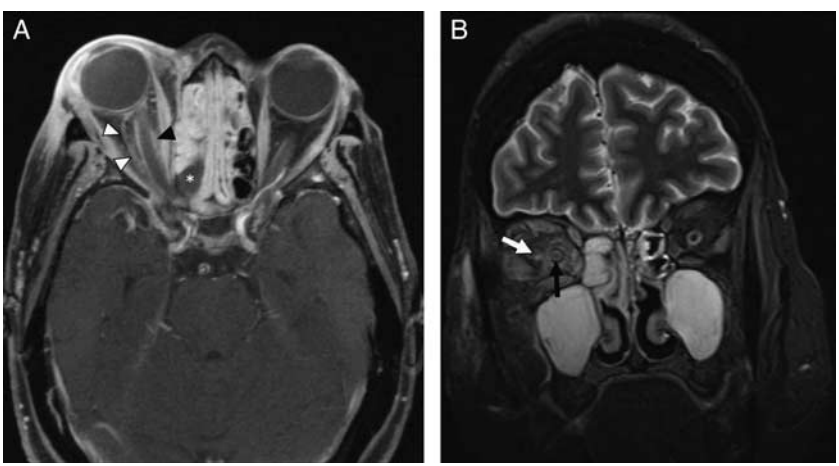

Figure 29. *60-year-old woman with CLL was admitted for febrile neutropenia developed right eye chemosis, periorbital edema, and proptosis. She was taken urgently for orbital extenteration, which revealed invasive fungal disease. Axial T1-weighted contrast-enhanced fat-saturated MRI (A) demonstrates absent enhancement of a right posterior ethmoid air cell (white asterisk) as well as heterogenous enhancement of the right optic nerve sheath (black arrow head) and intraconal fat (white arrow heads). Coronal T2-weighted MRI (B) demonstrates T2 hyperintensity of the right optic nerve (black arrow) and intraorbital fat (white arrow) consistent with orbital spread. CLL indicates chronic lymphocytic leukemia; MRI, magnetic resonance imaging.*

Angioinvasive Fungal Disease

Invasive fungal disease of the orbit typically occurs in immunocompromised or poorly controlled diabetic patients.[84] The primary site of infection is usually the sinuses with subsequent spread into the obit.[85] In addition to the signs and symptoms of sinusitis, patients with invasive fungal disease of the orbit present with optic neuropathy, trigeminal hypesthesia, and impaired ocular motility.[86] CT will demonstrate mucosal thickening of the involved sinuses with bony destruction and intraorbital extension of the inflammation.[84] The pathognomonic finding on MRI is absent sinus mucosal enhancement indicative of necrosis (Fig. 29). MRI is superior to CT in detecting intraorbital involvement and demonstrates enhancing inflammatory changes within the orbital fat and extraocular muscles (Fig. 29).[84] Even with early diagnosis, mortality rates are high and have been reported as high as 80%.[86]

The authors declare that they have no conflicts of interest to disclose.

■ References

1. Hasso AN, Drayer BP, Anderson RE, et al. Orbits, vision, and visual loss. American College of Radiology. ACR Appropriateness Criteria. *Radiology*. 2000;215(suppl):579–587.
2. Bhatti MT, Schmalfuss I. *Handbook of Neuroimaging for the Ophthalmologist*. London: JP Medical Ltd; 2014.
3. Winegar BA, Gutierrez JE. Imaging of orbital trauma and emergent non-traumatic conditions. *Neuroimaging Clin N Am*. 2015;25:439–456.
4. Damgaard OE, Larsen CG, Felding UA, et al. Surgical timing of the orbital "Blowout" fracture: a systematic review and meta-analysis. *Otolaryngol Head Neck Surg*. 2016;155: 387–390.
5. Bord SP, Linden J. Trauma to the globe and orbit. *Emerg Med Clin North Am*. 2008; 26:97–123. vi–vii.
6. Roth FS, Koshy JC, Goldberg JS, et al. Pearls of orbital trauma management. *Semin Plast Surg*. 2010;24:398–410.
7. Lima V, Burt B, Leibovitch I, et al. Orbital compartment syndrome: the ophthalmic surgical emergency. *Surv Ophthalmol*. 2009;54:441–449.
8. Winterton JV, Patel K, Mizen KD. Review of management options for a retrobulbar hemorrhage. *J Oral Maxillofac Surg*. 2007;65:296–299.
9. Fattahi T, Brewer K, Retana A, et al. Incidence of retrobulbar hemorrhage in the emergency department. *J Oral Maxillofac Surg*. 2014;72:2500–2502.
10. Kloss BT, Patel R. Orbital compartment syndrome from retrobulbar hemorrhage. *Int J Emerg Med*. 2010;3:521–522.
11. Wassef M, Blei F, Adams D, et al. Vascular anomalies classification: recommendations from the International Society for the Study of Vascular Anomalies. *Pediatrics*. 2015; 136:e203–e214.
12. Rubin PA, Remulla HD. Orbital venous anomalies demonstrated by spiral computed tomography. *Ophthalmology*. 1997;104:1463–1470.

13. Yazici B, Yazici Z, Gelisken O. An unusual case: bilateral orbital varices. *Acta Ophthalmol Scand*. 1999;77:453–455.
14. Gorospe L, Royo A, Berrocal T, et al. Imaging of orbital disorders in pediatric patients. *Eur Radiol*. 2003;13:2012–2026.
15. Bilaniuk LT. Orbital vascular lesions. Role of imaging. *Radiol Clin North Am*. 1999;37: 169–183. xi.
16. Smoker WR, Gentry LR, Yee NK, et al. Vascular lesions of the orbit: more than meets the eye. *Radiographics*. 2008;28:185–204; quiz 325.
17. Ansari SA, Mafee MF. Orbital cavernous hemangioma: role of imaging. *Neuroimaging Clin N Am*. 2005;15:137–158.
18. Ellis JA, Goldstein H, Connolly ES Jr, et al. Carotid-cavernous fistulas. *Neurosurg Focus*. 2012;32:E9.
19. Barrow DL, Spector RH, Braun IF, et al. Classification and treatment of spontaneous carotid-cavernous sinus fistulas. *J Neurosurg*. 1985;62:248–256.
20. Gupta AK, Purkayastha S, Krishnamoorthy T, et al. Endovascular treatment of direct carotid cavernous fistulae: a pictorial review. *Neuroradiology*. 2006;48:831–839.
21. Gemmete JJ, Chaudhary N, Pandey A, et al. Treatment of carotid cavernous fistulas. *Curr Treat Options Neurol*. 2010;12:43–53.
22. Chung EM, Murphey MD, Specht CS, et al. From the archives of the AFIP. Pediatric orbit tumors and tumorlike lesions: osseous lesions of the orbit. *Radiographics*. 2008; 28:1193–1214.
23. Reissis D, Pfaff MJ, Patel A, et al. Craniofacial dermoid cysts: histological analysis and inter-site comparison. *Yale J Biol Med*. 2014;87:349–357.
24. Pellerano F, Guillermo E, Garrido G, et al. Congenital orbital teratoma. *Ocul Oncol Pathol*. 2017;3:11–16.
25. Shields JA, Shields CL. Orbital cysts of childhood—classification, clinical features, and management. *Surv Ophthalmol*. 2004;49:281–299.
26. Yan J, Li Y, Chen Q, et al. Rare orbital cystic lesions in children. *J Craniomaxillofac Surg*. 2015;43:238–243.
27. Jurdy L, Merks JH, Pieters BR, et al. Orbital rhabdomyosarcomas: a review. *Saudi J Ophthalmol*. 2013;27:167–175.
28. Conneely MF, Mafee MF. Orbital rhabdomyosarcoma and simulating lesions. *Neuroimaging Clin N Am*. 2005;15:121–136.
29. Demirci H, Shields CL, Shields JA, et al. Orbital tumors in the older adult population. *Ophthalmology*. 2002;109:243–248.
30. Demirci H, Shields CL, Karatza EC, et al. Orbital lymphoproliferative tumors: analysis of clinical features and systemic involvement in 160 cases. *Ophthalmology*. 2008;115: 1626.e1–1631.e3.
31. Valvassori GE, Sabnis SS, Mafee RF, et al. Imaging of orbital lymphoproliferative disorders. *Radiol Clin North Am*. 1999;37:135–150. x–xi.
32. Nutting CM, Jenkins CD, Norton AJ, et al. Primary orbital lymphoma. *Hematol J*. 2002;3:14–16.
33. Bernardini FP, Bazzan M. Lymphoproliferative disease of the orbit. *Curr Opin Ophthalmol*. 2007;18:398–401.
34. Tailor TD, Gupta D, Dalley RW, et al. Orbital neoplasms in adults: clinical, radiologic, and pathologic review. *Radiographics*. 2013;33:1739–1758.
35. Sepahdari AR, Aakalu VK, Setabutr P, et al. Indeterminate orbital masses: restricted diffusion at MR imaging with echo-planar diffusion-weighted imaging predicts malignancy. *Radiology*. 2010;256:554–564.
36. Ahmad SM, Esmaeli B. Metastatic tumors of the orbit and ocular adnexa. *Curr Opin Ophthalmol*. 2007;18:405–413.
37. Valenzuela AA, Archibald CW, Fleming B, et al. Orbital metastasis: clinical features, management and outcome. *Orbit*. 2009;28:153–159.

38. Park WC, White WA, Woog JJ, et al. The role of high-resolution computed tomography and magnetic resonance imaging in the evaluation of isolated orbital neurofibromas. *Am J Ophthalmol*. 2006;142:456–463.
39. Ghosh PS, Ghosh D. Teaching neuroimages: MRI "target sign" and neurofibromatosis type 1. *Neurology*. 2012;78:e63.
40. Kransdorf MJ, Moser RP Jr, Gilkey FW. Fibrous dysplasia. *Radiographics*. 1990;10: 519–537.
41. Bhattacharya S, Mishra RK. Fibrous dysplasia and cherubism. *Indian J Plast Surg*. 2015;48:236–248.
42. Fitzpatrick KA, Taljanovic MS, Speer DP, et al. Imaging findings of fibrous dysplasia with histopathologic and intraoperative correlation. *AJR Am J Roentgenol*. 2004;182: 1389–1398.
43. Chong VF, Khoo JB, Fan YF. Fibrous dysplasia involving the base of the skull. *AJR Am J Roentgenol*. 2002;178:717–720.
44. LeBedis CA, Sakai O. Nontraumatic orbital conditions: diagnosis with CT and MR imaging in the emergent setting. *Radiographics*. 2008;28:1741–1753.
45. Kline LB, Hoyt WF. The Tolosa-Hunt syndrome. *J Neurol Neurosurg Psychiatry*. 2001;71: 577–582.
46. Goto Y, Hosokawa S, Goto I, et al. Abnormality in the cavernous sinus in three patients with Tolosa-Hunt syndrome: MRI and CT findings. *J Neurol Neurosurg Psychiatry*. 1990; 53:231–234.
47. Bahn RS. Graves' ophthalmopathy. *N Engl J Med*. 2010;362:726–738.
48. Kornreich L, Blaser S, Schwarz M, et al. Optic pathway glioma: correlation of imaging findings with the presence of neurofibromatosis. *AJNR Am J Neuroradiol*. 2001;22: 1963–1969.
49. Sylvester CL, Drohan LA, Sergott RC. Optic-nerve gliomas, chiasmal gliomas and neurofibromatosis type 1. *Curr Opin Ophthalmol*. 2006;17:7–11.
50. Cnossen MH, Stam EN, Cooiman LC, et al. Endocrinologic disorders and optic pathway gliomas in children with neurofibromatosis type 1. *Pediatrics*. 1997;100: 667–670.
51. Koeller KK, Rushing EJ. From the archives of the AFIP: pilocytic astrocytoma: radiologic-pathologic correlation. *Radiographics*. 2004;24:1693–1708.
52. Jackson A, Patankar T, Laitt RD. Intracanalicular optic nerve meningioma: a serious diagnostic pitfall. *AJNR Am J Neuroradiol*. 2003;24:1167–1170.
53. Deftereos SP, Karagiannakis GK, Spanoudaki A, et al. Optic nerve sheath meningioma: a case report. *Cases J*. 2008;1:423.
54. Saeed P, Rootman J, Nugent RA, et al. Optic nerve sheath meningiomas. *Ophthalmology*. 2003;110:2019–2030.
55. Kanamalla US. The optic nerve tram-track sign. *Radiology*. 2003;227:718–719.
56. Balcer LJ. Clinical practice. Optic neuritis. *N Engl J Med*. 2006;354:1273–1280.
57. Barnett Y, Sutton IJ, Ghadiri M, et al. Conventional and advanced imaging in neuromyelitis optica. *AJNR Am J Neuroradiol*. 2014;35:1458–1466.
58. Vaidhyanath R, Kirke R, Brown L, et al. Lacrimal fossa lesions: pictorial review of CT and MRI features. *Orbit*. 2008;27:410–418.
59. Mafee MF, Edward DP, Koeller KK, et al. Lacrimal gland tumors and simulating lesions. Clinicopathologic and MR imaging features. *Radiol Clin North Am*. 1999;37: 219–239. xii.
60. Bernardini FP, Devoto MH, Croxatto JO. Epithelial tumors of the lacrimal gland: an update. *Curr Opin Ophthalmol*. 2008;19:409–413.
61. Zhang F, Sha Y, Qian J, et al. Role of magnetic resonance diffusion-weighted imaging in differentiating lacrimal masses. *J Magn Reson Imaging*. 2014;40:641–648.
62. Andreasen S, Esmaeli B, Holstein SL, et al. An update on tumors of the lacrimal gland. *Asia Pac J Ophthalmol*. 2017;6:159–172.

63. Strianese D. Epithelial tumours of the lacrimal gland: a clinical, histopathological, surgical and oncological survey. *Acta Ophthalmol (Copenh)*. 2014;92:e79–e80.
64. Purohit BS, Vargas MI, Ailianou A, et al. Orbital tumours and tumour-like lesions: exploring the armamentarium of multiparametric imaging. *Insights Imaging*. 2016;7: 43–68.
65. Rasmussen P, Ralfkiaer E, Prause JU, et al. Malignant lymphoma of the lacrimal gland: a nation-based study. *Arch Ophthalmol*. 2011;129:1275–1280.
66. Politi LS, Forghani R, Godi C, et al. Ocular adnexal lymphoma: diffusion-weighted MR imaging for differential diagnosis and therapeutic monitoring. *Radiology*. 2010; 256:565–574.
67. Koyama T, Ueda H, Togashi K, et al. Radiologic manifestations of sarcoidosis in various organs. *Radiographics*. 2004;24:87–104.
68. Smith JK, Matheus MG, Castillo M. Imaging manifestations of neurosarcoidosis. *AJR Am J Roentgenol*. 2004;182:289–295.
69. Yanardag H, Pamuk ON. Lacrimal gland involvement in sarcoidosis. The clinical features of 9 patients. *Swiss Med Wkly*. 2003;133:388–391.
70. Mafee MF, Dorodi S, Pai E. Sarcoidosis of the eye, orbit, and central nervous system. Role of MR imaging. *Radiol Clin North Am*. 1999;37:73–87. x.
71. Tan LT, Davagnanam I, Isa H, et al. Clinical and imaging features of lacrimal gland involvement in granulomatosis with polyangiitis. *Ophthalmology*. 2015;122:2125–2129.
72. Lanza JT, Ku Y, Lucente FE, et al. Wegener's granulomatosis of the orbit: lacrimal gland involvement as a major sign. *Am J Otolaryngol*. 1995;16:119–122.
73. Nwawka OK, Nadgir R, Fujita A, et al. Granulomatous disease in the head and neck: developing a differential diagnosis. *Radiographics*. 2014;34:1240–1256.
74. Patel R, Shahane A. The epidemiology of Sjogren's syndrome. *Clin Epidemiol*. 2014;6:247–255.
75. Tonami H, Matoba M, Yokota H, et al. CT and MR findings of bilateral lacrimal gland enlargement in Sjogren syndrome. *Clin Imaging*. 2002;26:392–396.
76. Kawai Y, Sumi M, Kitamori H, et al. Diffusion-weighted MR microimaging of the lacrimal glands in patients with Sjogren's syndrome. *AJR Am J Roentgenol*. 2005;184: 1320–1325.
77. Mombaerts I, Schlingemann RO, Goldschmeding R, et al. The surgical management of lacrimal gland pseudotumors. *Ophthalmology*. 1996;103:1619–1627.
78. Andrew NH, Kearney D, Sladden N, et al. Idiopathic dacryoadenitis: clinical features, histopathology, and treatment outcomes. *Am J Ophthalmol*. 2016;163:148.e1–153.e1.
79. Platnick J, Crum AV, Soohoo S, et al. The globe: infection, inflammation, and systemic disease. *Semin Ultrasound CT MR*. 2011;32:38–50.
80. Block SL. Getting an eyeful of preseptal cellulitis. *Pediatr Ann*. 2013;42:99–102.
81. Eustis HS, Mafee MF, Walton C, et al. MR imaging and CT of orbital infections and complications in acute rhinosinusitis. *Radiol Clin North Am*. 1998;36:1165–1183. xi.
82. Ludwig BJ, Foster BR, Saito N, et al. Diagnostic imaging in nontraumatic pediatric head and neck emergencies. *Radiographics*. 2010;30:781–799.
83. Dankbaar JW, van Bemmel AJ, Pameijer FA. Imaging findings of the orbital and intracranial complications of acute bacterial rhinosinusitis. *Insights Imaging*. 2015;6: 509–518.
84. Aribandi M, McCoy VA, Bazan C III. Imaging features of invasive and noninvasive fungal sinusitis: a review. *Radiographics*. 2007;27:1283–1296.
85. Farooq AV, Patel RM, Lin AY, et al. Fungal orbital cellulitis: presenting features, management and outcomes at a referral center. *Orbit*. 2015;34:152–159.
86. Trief D, Gray ST, Jakobiec FA, et al. Invasive fungal disease of the sinus and orbit: a comparison between mucormycosis and Aspergillus. *Br J Ophthalmol*. 2016;100:184–188.